

## Electromagnetic instabilities and current structures in anisotropic superconductors

A. Gurevich

*Kernforschungszentrum Karlsruhe, Institut für Technische Physik, Postfach 3640, D-7500 Karlsruhe, Germany  
and Applied Superconductivity Center, University of Wisconsin, Madison, Wisconsin 53706\**

(Received 22 October 1991)

Electromagnetic instability of uniform current flow in anisotropic type-II superconductors has been considered. It is shown that the instability occurs in the region  $j_{f1} < j < j_{f2}$ , essentially depending on the orientation of the current density  $\mathbf{j}$  with respect to the symmetry axes. This is due to the coupling of the anisotropy and strong nonlinearity of the  $I$ - $V$  curve in the flux-creep regime, regardless of specific mechanisms of flux dynamics. Peculiarities of the instability in different models of resistive states (conventional flux-creep model, vortex glass, critical-state model, etc.) are examined. The instability is shown to destroy laminar current configurations and is accompanied by the appearance of current domain walls and macroscopic-vortex current patterns, which depend on the sample geometry. A qualitative description of the macroscopic vortex structures is given, and their manifestations in electric and magnetic properties of anisotropic superconductors are discussed.

### I. INTRODUCTION

Vortex structures in anisotropic type-II superconductors reveal a number of characteristic features as compared to the isotropic case, for example, a noncollinearity of flux lines and applied magnetic field  $\mathbf{H}$ , noncentral forces upon vortices and their attraction along certain crystallographic directions,<sup>1</sup> existence of quasi-two-dimensional (2D) vortices localized at superconducting planes in layered materials,<sup>2,3</sup> etc. The anisotropy considerably reduces the tilt and shear elastic moduli of the flux-line lattice (FLL) and, as a consequence, the energies of defects (vortex loops, kinks, dislocations, etc.) arising in the mixed state.<sup>4,5</sup> The latter proves to be especially important for anisotropic high- $T_c$  superconductors due to high operating temperatures and low line tension of a fluxon, which leads to significant fluctuations of vortex positions, thermally activated generation of defects in the FLL, entanglement and reconnection of vortices, etc.<sup>5,6</sup> In other words, the anisotropy generally reduces the stability of the FLL with respect to the generation of defects, which (together with high  $T_c$  and relatively weak pinning<sup>7</sup>) leads to a fast relaxation of irreversible magnetization and low critical current density  $j_c$ . In addition, the high density of defects can cause some instabilities of the Abrikosov FLL, resulting in its transition into states such as liquid phases,<sup>4,6</sup> vortex glass,<sup>8</sup> etc. In this case, the effect of the anisotropy does not reduce to a renormalization of parameters and their angular dependences only (see, e.g., Ref. 9), but also can facilitate the appearance of new flux structures and lead to specific instabilities of the FLL.

In the presence of a macroscopic current  $I$ , vortex structures become metastable, which manifests itself in a decay of an induced  $I(t)$  due to thermal fluctuations (flux creep). In this case the anisotropy affects the stability not only on the level of individual vortices, but also via a macroscopic electric field  $\mathbf{E}(r,t)$  generated by the flux

creep. As a result, the stability of the mixed state becomes dependent on dissipative processes as well, in particular, on the form of current-voltage ( $I$ - $V$ ) characteristic of a superconductor. For nonlinear resistive states the anisotropy can considerably restrict possible forms of  $I$ - $V$  curves for which uniform current flow is stable to small electromagnetic perturbations. Here the coupling of anisotropy and nonlinearity of  $I(V)$  can lead to a collective electromagnetic instability of the vortex system since one of the principal values of the differential resistivity tensor  $R_{\alpha\beta}$  becomes negative for current densities  $j_{f1} < j < j_{f2}$  essentially depending upon the orientation of  $\mathbf{j}$  with respect to the symmetry axes.<sup>10</sup>

The instability occurs provided that the nonlinearity of  $I(V)$  and/or the anisotropy is high enough. The strong nonlinearity of  $I(V)$  in the flux-creep regime ( $j < j_c$ ) is typical for any hard superconductor having the  $I$ - $V$  curve similar to that shown in Fig. 1. At the same time, the essential anisotropy is a characteristic feature of high- $T_c$  superconductors for which such an instability could easily be realized. The corresponding instability criteria can be expressed in terms of directly measured parameters, regardless of the microstructure of the mixed state as well as specific mechanisms of flux dynamics and pinning. One can be shown<sup>10</sup> that the anisotropy results in the instability of some models which had originally been proposed for isotropic superconductors and then were applied to the anisotropic case by taking account of angular dependences of parameters. For instance, such a situation occurs for the Bean critical-state model with an anisotropic  $j_c$ ,<sup>11</sup> vortex glass<sup>8</sup> and collective creep<sup>12</sup> models, conventional flux-creep model,<sup>13</sup> etc. Here the anisotropy can lead to a qualitative transformation of the FLL and appearance of new nonuniform states which cannot exist in isotropic superconductors. Notice that the instability results from a resistive part of  $\mathbf{j}$  which is usually small as compared with the nondissipative  $j_c$  in a region of the phase diagram below the irreversibility line.<sup>14</sup> In

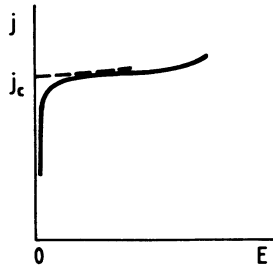


FIG. 1. Typical  $I$ - $V$  curve for a type-II hard superconductor.

isotropic superconductors this justifies the use of the critical state concept which is valid provided that  $k_B T \ll U$ , where  $U$  is an apparent flux-creep activation energy.<sup>13</sup> However, in anisotropic superconductors the situation changes qualitatively, since just the small resistive part of  $\mathbf{j}$  can lead to the instability even if  $k_B T/U \ll 1$ . As a result, the use of the critical-state model in anisotropic superconductors may require a stability analysis for each specific case, depending on the sample geometry, induced electric fields, and details of  $I$ - $V$  curves in the flux-creep regime.

The instability leads to macroscopic spatial modulations of magnetic flux and current since one of the principal values of magnetic diffusivity tensor  $D_{\alpha\beta} = \mu_0^{-1} R_{\alpha\beta}$  becomes negative along a direction which coincides with neither the symmetry axes nor the current direction. This is a manifestation of an instability of nonlinear current flow in anisotropic media with respect to a local turn of the initial  $\mathbf{j}(\mathbf{r})$  toward a new direction corresponding to a lower resistance. However, the uniform turn of current is usually incompatible with the boundary conditions ensuring zero normal components of  $\mathbf{j}(\mathbf{r})$  at the lateral surface of a sample. This results in a partial closure of current lines and appearance of current patterns which depend upon the sample geometry. Depending on the value and orientation of  $\mathbf{j}$ , such patterns can vary from weak modulations of an initially uniform  $\mathbf{j}$  to cellular current structures consisting of an array of magnetic macroscopic vortices in the system of Abrikosov vortices.<sup>10</sup> In this case, the anisotropy results in a dissipative transition from laminar into some "turbulent" current flow. Such a transition may be considered as an analog of the field-induced orientational instability arising in liquid crystals, where the electric or magnetic field can lead to a spontaneous generation of domain walls separating regions with different orientation of the director, or the appearance of dynamic vortex structures (see, e.g., Ref. 15).

Therefore, the anisotropy reduces the stability of the mixed state on both the macroscopic and microscopic scales, which can lead to novel flux structures. In this paper, I focus only on the macroscopic level and consider the electromagnetic instability of uniform current flow and the appearance of current patterns in anisotropic superconductors. Within the framework of the macroscopic approach,<sup>10</sup> the instability results from the coupling of the anisotropy and the strong nonlinearity of  $I(V)$  caused

by the nonzero  $j_c$  (Fig. 1), regardless of microscopic mechanisms of flux dynamics. For that reason I shall not discuss in detail temperature and field dependences of characteristic critical currents which can be essentially model dependent. Instead, a general instability criterion obtained is illustrated by different models of flux dynamics in order to reveal some universal features of the instability which can be formulated as a kinetic phase transition. The latter enables one to use the universal scheme which has been developed for a description of equilibrium phase transitions. Here we restrict ourselves to a qualitative analysis of the macroscopic vortex structures arising above the instability threshold. It will be shown that there is a mathematical analogy of the nonlinear Maxwell equations describing the macroscopic vortex current structure with equations describing a supersonic gas flow. This enables one to predict the appearance of discontinuities of current flow in anisotropic superconductors analogous to the shock waves in aerodynamics.

The paper is organized as follows. In Sec. II, the stability of uniform current flow to small electromagnetic perturbations is considered. The analysis is based on general properties of  $I$ - $V$  curves in anisotropic superconductors and restrictions imposed by symmetry. An explicit instability criterion is obtained; the geometry of the instability and its dependence upon the current direction is analyzed. Peculiarities of the instability in various models of resistive states (single-vortex and collective flux-creep, vortex glass, critical-state models, etc.) are discussed as an illustration. Section III is devoted to nonlinear current structures caused by the instability. Qualitative analysis of low-amplitude current patterns and macroscopic-vortex structures are given. The instability is formulated as a spinodal decomposition of the uniform resistive state due to a kinetic phase transition from a laminar to vortical flux-creep regimes. By using a hodograph transformation of the Maxwell equations, a quasihydrodynamic approach is proposed for description of stationary current configurations in anisotropic superconductors. Section IV contains a discussion of the results and possible manifestations of the instability in magnetic and electric properties of anisotropic superconductors. The relation of the macroscopic vortex structure to the observed magnetic granularity of nonceramic high- $T_c$  oxides is discussed.

## II. LINEAR STABILITY OF UNIFORM CURRENT FLOW

### A. Symmetry of $I$ - $V$ Curves

We begin first with an analysis of nonlinear  $I$ - $V$  curves in anisotropic superconductors assuming for simplicity the rhombic crystalline symmetry with the orthogonal symmetry axes  $x$ ,  $y$ , and  $z$ . In the case of an arbitrary orientation of the magnetic induction  $\mathbf{B}$  with respect to  $x$ ,  $y$ , and  $z$ , the electric field  $\mathbf{E}$  is not parallel to the current density  $\mathbf{j}$ , therefore the  $I$ - $V$  characteristic can be presented in the form

$$\mathbf{E} = \mathbf{G}(\mathbf{j}, \mathbf{B}), \quad (2.1)$$

where  $\mathbf{G}(\mathbf{j}, \mathbf{B})$  is a nonlinear vector function obeying the relations

$$\mathbf{G}(\mathbf{j}, \mathbf{B}) = -\mathbf{G}(-\mathbf{j}, \mathbf{B}) = -\mathbf{G}(\mathbf{j}, -\mathbf{B}) = \mathbf{G}(-\mathbf{j}, -\mathbf{B}),$$

provided that the crystal is invariant under inversion and the Hall effect is negligible. Unlike the isotropic case, the anisotropy leads to a noncollinearity of  $\mathbf{E}$  and  $\mathbf{j}$  even for  $\mathbf{j} \perp \mathbf{B}$ . For  $\mathbf{B}$  parallel to one of the symmetry axis (say, the  $z$  axis) the vectors  $\mathbf{j}$  and  $\mathbf{E}$  lie in the  $xy$  plane and Eq. (2.1) reduces to

$$E_x = G_x(j, \phi), \quad E_y = G_y(j, \phi), \quad (2.2)$$

where  $\phi$  is the angle of  $\mathbf{j}$  with the  $x$  axis,  $j_x = j \cos \phi$ ,  $j_y = j \sin \phi$ ,  $j = |\mathbf{j}|$ . In this case the invariance under inversion results in that  $E_y = 0$  at  $j_y = 0$  and  $E_x = 0$  at  $j_x = 0$ , in other words,  $G_y(\phi) = 0$ ,  $\partial G_x / \partial \phi = 0$  at  $\phi = (0, \pi)$ , and  $G_x(\phi) = 0$ ,  $\partial G_y / \partial \phi = 0$  at  $\phi = \mp \pi/2$ .

In general, the angle  $\Psi$  between  $\mathbf{E}$  and  $\mathbf{x}$  depends on both  $\phi$  and  $j$ . If, by analogy with linear media, one regards  $\Psi$  to be independent of  $j$ , the  $I$ - $V$  curve takes the form

$$E_{\alpha\beta} = \rho_{\alpha\beta} j_{\beta} G(j, \phi), \quad (2.3)$$

where  $\rho_{\alpha\beta}$  is a linear resistivity tensor,  $G$  is a function of  $j$  and  $\phi$ , and  $\alpha, \beta \in (x, y, z)$ . In this case, the principal axes of  $\rho_{\alpha\beta}$  coincide with  $x$ ,  $y$ , and  $z$ ; moreover,  $\cot \Psi = (\rho_x / \rho_y) \cot \phi$  at  $j_z = 0$ , where  $\rho_x$  and  $\rho_y$  are the principal values of  $\rho_{\alpha\beta}$ . Furthermore,

$$\frac{\partial G}{\partial \phi} = 0, \quad \phi = \frac{\pi n}{2}, \quad n = 0, \pm 1, \pm 2, \quad (2.4)$$

due to the invariance under inversion. The quantities  $\rho_{\alpha\beta}$  and  $G$  will be clarified below. The use of Eq. (2.3) instead of general Eq. (2.2) can be justified, if one takes into account the strong nonlinearity of  $I(V)$  at  $j < j_c$  due to the flux creep which manifests itself as a macroscopic motion of some fraction of magnetic flux  $G$  which essentially depends on  $j$  [in various models  $G$  depends on  $j$  exponentially or as  $j^m$  with  $m \gg 1$  (Refs. 8, 12, 13, 16, and 17)]. Since just that motion causes the electric field  $\mathbf{E}$ , hence, it follows that formula (2.3) can be considered as a general relation between the vectors  $\mathbf{E}$  and  $\mathbf{j}$ , where the components  $\rho_{\alpha\beta}$  play the role of kinetic coefficients whose relatively weak dependence on  $j$  (see, e.g., Ref. 18) can be neglected as compared to the scalar function  $G(j, \phi)$ . Therefore, formula (2.3) takes into account main qualitative features caused by the anisotropy, namely, the noncollinearity of  $\mathbf{j}$  and  $\mathbf{E}$  and the angular dependence of a mean density of depinned vortices proportional to  $G(j, \phi)$ . For this reason I shall use just Eq. (2.3) instead of the more complicated Eq. (2.2), which enables one to simplify considerably the exposition.

### B. Instability criterion

In this paper we consider an instability of uniform resistive state caused by negative components of the differential resistivity tensor  $R_{\alpha\beta} = \partial E_{\alpha} / \partial j_{\beta}$ . This implies that, at the instability threshold, a principal value of the tensor  $R_{\alpha\beta}$  vanishes for one of its principal axes  $\zeta$ ,  $\eta$ ,

and  $\xi$ , whose orientations are determined by the orthogonal eigenvectors  $\mathbf{n}_p$ , where  $p = (\zeta, \eta, \xi)$ . Notice that for nonlinear anisotropic media, the vectors  $\mathbf{n}_p(\mathbf{j})$  essentially depend on  $\mathbf{j}$  and generally coincide with neither the symmetry axes ( $x, y, z$ ) nor the current direction. The stability analysis of the dissipative current flow to small electromagnetic perturbations  $\delta \mathbf{E}(\mathbf{r}, t)$  and  $\delta \mathbf{B}(\mathbf{r}, t)$  can be carried out by means of the Maxwell equations  $\partial_t \delta \mathbf{B} = -\text{curl} \delta \mathbf{E}$ ,  $\text{curl} \delta \mathbf{H} = \delta \mathbf{j}$ , and  $\delta E_{\alpha} = R_{\alpha\beta} \delta j_{\beta}$ . If one neglects the self-field effects,<sup>19</sup> the Maxwell equations reduce to a set of linear equations

$$i\omega \mu_0 \delta \mathbf{j}(\mathbf{k}) = [\mathbf{k} \times [\mathbf{k} \times \delta \mathbf{E}(\mathbf{k})]]$$

and  $\delta E_{\alpha}(\mathbf{k}) = R_{\alpha\beta} \delta j_{\beta}(\mathbf{k})$  for the Fourier components

$$\delta \mathbf{E}(\mathbf{k}, \omega) = \int \delta \mathbf{E}(\mathbf{r}, t) \exp(-i\omega t - i\mathbf{k} \cdot \mathbf{r}) d^3 r dt,$$

$$\delta \mathbf{j}(\mathbf{k}, \omega) = \int \delta \mathbf{j}(\mathbf{r}, t) \exp(-i\omega t - i\mathbf{k} \cdot \mathbf{r}) d^3 r dt.$$

Hereafter, we put, for simplicity,  $\mathbf{B} = \mu_0 \mathbf{H}$ , which corresponds to  $H_{c1} \ll H \ll H_{c2}$  and  $H_{c1}$  and  $H_{c2}$  the lower and upper critical fields, respectively. The condition of solvability of the algebraic equations for  $\delta \mathbf{E}(\mathbf{k}, \omega)$  yields the following dispersion relation for the increment  $\lambda = i\omega$  which depends on the orientation of the wave vector  $\mathbf{k}$

$$\lambda(\mathbf{k}) = -\mu_0^{-1} k^2 f(\mathbf{n}). \quad (2.5)$$

This formula gives the spectrum of electromagnetic perturbations  $\delta \mathbf{E}(\mathbf{r}, t) \propto \exp(\lambda t + i\mathbf{k} \cdot \mathbf{r})$  in an infinite medium, where  $\mathbf{n} = \mathbf{k}/k$  is the unit vector along  $\mathbf{k}$ , and  $k = |\mathbf{k}|$ . The function  $f(\mathbf{n})$  obeys the following secular equation:

$$\det[R_{\alpha\beta} - n_{\alpha} n_{\gamma} R_{\gamma\beta} - f \delta_{\alpha\beta}] = 0, \quad (2.6)$$

where  $\delta_{\alpha\beta}$  is the Kronecker symbol. The instability occurs if Eq. (2.6) has solutions with  $\text{Re} f(\mathbf{n}) < 0$  corresponding to the exponential growth of electromagnetic perturbations with  $t$ . This is equivalent to that one of the principal values of  $R_{\alpha\beta}$  becomes negative. In the case of an arbitrary orientation of  $\mathbf{j}$  with respect to the symmetry axes, Eq. (2.6) reduces to a cumbersome quadratic equation for  $f(\mathbf{n})$  given in Appendix A. For this reason we consider here a simpler case of the 2D instability for which the vectors  $\mathbf{j}$  and  $\mathbf{E}$  have only the  $x$  and  $y$  components. This enables one to get an explicit instability criterion valid for both thin films and 3D anisotropic superconductors if the current flows along the symmetry planes ( $\mathbf{B} \parallel \mathbf{z}$ ,  $\mathbf{j} \parallel xy$ ).

For the 2D case, the perturbations  $\delta \mathbf{H}(\mathbf{r}, t)$  have only the  $z$  component  $\delta H$ , and the Maxwell equations reduce to

$$\partial_t \delta B = \partial_y \delta E_x - \partial_x \delta E_y, \quad (2.7a)$$

$$\delta j_x = \partial_y \delta H, \quad \delta j_y = -\partial_x \delta H. \quad (2.7b)$$

Inserting  $\delta E_{\alpha} = R_{\alpha\beta} \delta j_{\beta}$  into Eqs. (2.7), one gets the following equation for  $\delta H$ :

$$\mu_0 \partial_t \delta H = [R_{yy} \partial_{xx} + (R_{xy} + R_{yx}) \partial_{xy} + R_{xx} \partial_{yy}] \delta H, \quad (2.8)$$

which describes different modes  $\delta H(\mathbf{k}) \propto \exp(\lambda t + i\mathbf{k} \cdot \mathbf{r})$ , where  $\lambda(\mathbf{k})$  is given by Eq. (2.5) and

$$f(\mathbf{n}) = R_{yy}n_x^2 + (R_{xy} + R_{yx})n_x n_y + R_{xx}n_y^2. \quad (2.9)$$

The uniform state becomes unstable if there exists a direction  $\mathbf{n}$  for which  $\text{Re}\lambda(\mathbf{k}) > 0$ , i.e., the quadratic form (2.9) is negative. This condition first satisfies for the mode that has the minimum value of  $f(\mathbf{n})$ . The mode is unstable if  $f(\psi) < 0$  and  $\partial f / \partial \psi = 0$ , where we put  $n_x = \sin\psi$  and  $n_y = \cos\psi$ . Using these conditions, one finds, after a simple calculation, the instability criterion and the angle  $\psi$ , determining the propagation of the critical mode, in the form

$$4R_{xx}R_{yy} < (R_{xy} + R_{yx})^2, \quad (2.10)$$

$$\tan 2\psi = (R_{xy} + R_{yx}) / (R_{yy} - R_{xx}). \quad (2.11)$$

The angle  $\psi$  fixed by Eq. (2.11) also determines the orientation of the orthogonal principal axes  $\eta$  and  $\zeta$  of the tensor  $R_{\alpha\beta}$  in the  $xy$  plane because the minimization of the quadratic form (2.9) just gives two eigenvectors of  $R_{\alpha\beta}$ , one of them being directed along  $\mathbf{n}$  at  $f(\mathbf{n}) = 0$ . Let  $\mathbf{n}$  be parallel to  $\eta$ , then  $\zeta$  and  $\eta$  are related to  $x$  and  $y$  as follows:

$$\eta = y \cos\psi + x \sin\psi, \quad \zeta = y \sin\psi - x \cos\psi. \quad (2.12)$$

In the coordinate frame  $\zeta, \eta$ , Eq. (2.8) becomes

$$\mu_0 \partial_t \delta H = (R_1 \partial_{\zeta\zeta} + R_2 \partial_{\eta\eta}) \delta H, \quad (2.13)$$

where the principal values  $R_{1,2}$  are given by

$$2R_{1,2} = R_{xx} + R_{yy} \pm [(R_{xy} + R_{yx})^2 + (R_{xx} - R_{yy})^2]^{1/2}. \quad (2.14)$$

As follows from Eqs. (2.13) and (2.14), the instability criterion (2.10) implies that the principal value  $R_2$  along the  $\zeta$  axis perpendicular to  $\mathbf{n}$  becomes negative. The geometry of the instability is shown in Fig. 2. Formulas (2.10) and (2.11) are valid for 3D anisotropic supercon-

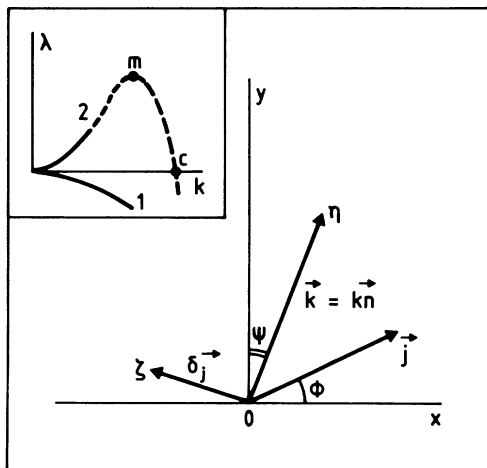


FIG. 2. Geometry of the instability. Inset: the spectrum  $\lambda(k)$  in the case  $s < s_c$  (curve 1) and  $s > s_c$  (curve 2). The dashed curve shows the modification of  $\lambda(k)$  due to the spatial dispersion of  $R_{\alpha\beta}$  (see text).

ductors as well, where the negative principal value  $R_2$  at  $\mathbf{B} \parallel \mathbf{z}$ ,  $\mathbf{j} \parallel \mathbf{xy}$  results in the instability in the  $xy$  plane.<sup>10</sup>

In anisotropic superconductors the criterion (2.10) can easily hold because of the strong nonlinearity of  $I(V)$  (Fig. 1). In order to show that, we calculate the elements  $R_{\alpha\beta}$  by differentiation of Eq. (2.3), which yields

$$\begin{aligned} R_{xx} &= \left[ G + j \cos^2\phi \frac{\partial G}{\partial j} - \cos\phi \sin\phi \frac{\partial G}{\partial \phi} \right] \rho_x, \\ R_{xy} &= \left[ j \cos\phi \sin\phi \frac{\partial G}{\partial j} + \cos^2\phi \frac{\partial G}{\partial \phi} \right] \rho_x, \\ R_{yx} &= \left[ j \cos\phi \sin\phi \frac{\partial G}{\partial j} - \sin^2\phi \frac{\partial G}{\partial \phi} \right] \rho_y, \\ R_{yy} &= \left[ G + j \sin^2\phi \frac{\partial G}{\partial j} + \cos\phi \sin\phi \frac{\partial G}{\partial \phi} \right] \rho_y, \end{aligned} \quad (2.15)$$

where  $\rho_x$  and  $\rho_y$  are the principal values of  $\rho_{\alpha\beta}$ . An explicit instability criterion can be obtained if one assumes the simplest scaling of the form  $G(j, \phi) = G(j/j_k(\phi))$  [the angular dependence of  $j_k(\phi)$  will be discussed below]. In this case, one has  $\partial G / \partial j = G' / j_k$ ,  $\partial G / \partial \phi = -u G' / j_k$ ,  $u = j / j_k$ ,  $G' = dG / du$ , therefore formulas (2.10) and (2.15) reduce to a quadratic inequality for  $G'$ . After some algebra the instability criterion (2.10) can be presented in the form

$$s(j) > s_c(\phi) = g/2 + (g^2/4 + g)^{1/2}, \quad (2.16)$$

where

$$g(\phi) = \frac{16\rho_x\rho_y}{[(\rho_x + \rho_y)b + (\rho_x - \rho_y)(b \cos 2\phi - \sin 2\phi)]^2}, \quad (2.17)$$

$$s(j) = \frac{\partial \ln G}{\partial \ln j}, \quad b(\phi) = \frac{\partial \ln j_k}{\partial \phi}. \quad (2.18)$$

Here the parameters  $s_c(\phi)$  and  $s(j, \phi)$  characterize the anisotropy and nonlinearity of  $I(V)$ , respectively, with  $s_c(\phi)$  being independent of  $j$ . Likewise, the angle  $\psi$  can be found from Eqs. (2.11) and (2.15) as follows:

$$\tan 2\psi = \frac{(\rho_x - \rho_y)b + (\rho_x + \rho_y)(b \cos 2\phi - \sin 2\phi)}{(\rho_x - \rho_y)(1 + 2/s) + (\rho_x + \rho_y)(\cos 2\phi + b \sin 2\phi)}. \quad (2.19)$$

Formulas (2.16)–(2.19) are the main results of the linear stability analysis for the  $I-V$  curve of the form (2.3). For instance, in the isotropic case ( $\rho_x = \rho_y$ ,  $b = 0$ ,  $g = \infty$ ), the inequality (2.16) does not hold for any  $s(j)$ , which implies that the resistive state is always stable to small electromagnetic perturbations. The anisotropy can change the situation qualitatively if the  $I-V$  curve is nonlinear ( $s > 0$ ). Indeed, since the right side of Eq. (2.16) does not depend on  $j$ , the criterion (2.16) can hold provided that the nonlinearity of  $I(V)$  or/and the anisotropy is strong enough. As follows from Eq. (2.17), there are two factors

resulting in the finite value of  $s_c(\phi)$  in anisotropic superconductors. The first one is the noncollinearity of  $\mathbf{j}$  and  $\mathbf{E}$  because of  $\rho_x \neq \rho_y$ , whereas the second one comes from the angular dependence of  $j_k$  ( $b \neq 0$ ), or, in other words, from the dependence of the fraction of the depinned flux on current direction.

As seen from Eqs. (2.8) and (2.13), the evolution of magnetic perturbations  $\delta H(\mathbf{r}, t)$  is described by a diffusive-type equation with the diffusivity tensor  $D_{\alpha\beta} = \mu_0^{-1} R_{\alpha\beta}$ . The condition  $R_2 = 0$  determines the instability threshold at which the principal value of  $D_{\alpha\beta}$  along the  $\xi$  axis vanishes, which leads to a spontaneous growth of magnetic flux structures at  $s > s_c$ . Similar phenomena arise in any system with negative differential resistivity which results in a stratification of uniform current flow into current domains or channels, as it takes place in semiconductors (Gunn instability),<sup>20</sup> hot plasma,<sup>21</sup> normal metals and superconductors,<sup>22</sup> etc. These phenomena are usually due to a bistability caused by nonequilibrium processes, which leads to the appearance of dissipative structures.<sup>21</sup> By contrast, the instability discussed in this paper is a result of the coupling of strong nonlinearity of  $I(V)$  and anisotropy and is not due to a renormalization of kinetic coefficients by nonequilibrium processes.<sup>23</sup>

### C. Examples

The instability criterion (2.16) can hold in various models of flux dynamics at anisotropy level typical for high- $T_c$  oxides. For instance, for the Anderson-Kim flux-creep model,<sup>13</sup> the  $I-V$  characteristics can be presented in the form

$$E_\alpha = \rho_{\alpha\beta} j_\beta \frac{j_1(\phi)}{j} \sinh \frac{j}{j_1(\phi)}. \quad (2.20)$$

Here  $j_1(\phi) = k_B T j_c(\phi) / U(\phi)$ ,  $U$  is an activation energy,  $\rho_{\alpha\beta}$  is the resistivity tensor in the thermally assisted flux-flow (TAFF) mode.<sup>24</sup> Formula (2.20) is the simplest generalization of the conventional flux-creep model which takes into account the anisotropy via the tensor  $\rho_{\alpha\beta}$  and the dependence of  $j_1(\phi)$  on current direction. By comparing Eqs. (2.3) and (2.20), one finds  $G(u) = (\sinh u) / u$ ,  $u = j / j_1$ , whence the criterion (2.16) can be written as

$$\frac{j}{j_1} \coth \frac{j}{j_1} - 1 > s_c(\phi). \quad (2.21)$$

In this model the nonlinearity of  $\mathbf{E}(\mathbf{j})$  increases with  $j$ , therefore the instability occurs at  $j > j_{f1}$ , where the value of  $j_{f1}$  in two limiting cases  $g \gg 1$  and  $g \ll 1$  is given by

$$j_{f1} = \begin{cases} gj_1, & g \gg 1, \\ \sqrt{3}g^{1/4}j_1, & g \ll 1. \end{cases} \quad (2.22)$$

$$j_{f1} = \begin{cases} gj_1, & g \gg 1, \\ \sqrt{3}g^{1/4}j_1, & g \ll 1. \end{cases} \quad (2.23)$$

Now we consider an anisotropic critical-state model<sup>11</sup> for which it is convenient to present  $\mathbf{E}(\mathbf{j})$  as follows:

$$E_\alpha = [1 - j_c(\phi) / j] \rho_{\alpha\beta} j_\beta, \quad (2.24)$$

where the  $I-V$  characteristic at  $j > j_c$  is assumed to be

linear,  $j_c(\phi)$  is an angular-dependent critical current density,  $\rho_{\alpha\beta}$  is a flux-flow resistivity tensor. In this case one has  $G = 1 - j_c / j$ , hence,  $s = j_c / (j - j_c)$ , and Eq. (2.16) reduces to  $j < j_{f2}$  with

$$j_{f2} = [(\frac{1}{4} + 1/g)^{1/2} + \frac{1}{2}] j_c. \quad (2.25)$$

From Eqs. (2.22) and (2.25), one finds that  $j_{f1} \sim j_1$  and  $j_{f2} \sim j_c$  in the case of strong anisotropy ( $g \sim 1$ ), which gives  $j_{f1} \sim (k_B T / U) j_c \ll j_{f2}$  in a region of the phase diagram below the irreversibility line  $U \gg k_B T$ .<sup>14</sup> At  $j_{f1} \ll j_{f2}$ , the values  $j_{f1,2}$  can be found, regardless of the crossover region between the flux-flow and flux-creep regimes, which was assumed above when deriving Eqs. (2.21) and (2.25).

Formulas (2.20) and (2.24) are some approximations of real  $I-V$  curves of anisotropic superconductors in flux-creep ( $j_c - j \gg j_1$ ) and flux-flow ( $j - j_c \gg j_1$ ) regimes, respectively. Other variants which have commonly been discussed in the literature involve, for example, the power  $I-V$  curve  $V \propto j^m$  with  $m \gg 1$ ,<sup>16,17</sup> nonlinear flux flow,<sup>18</sup>  $I-V$  curve of the form  $V \propto \exp[-(j_k / j)^\mu]$  predicted by vortex glass<sup>8</sup> and collective creep<sup>12</sup> modes, etc. For  $V \propto \exp[-(j_k / j)^\mu]$  the nonlinearity of  $\mathbf{E}(\mathbf{j})$  increases as  $j$  decreases, and  $s = \mu(j_k / j)^\mu$ . As a result, the criterion (2.16) holds if

$$j < j_g = j_k (\mu / s_c)^{1/\mu}, \quad (2.26)$$

where the parameter  $s_c$  involves all relevant mechanisms of anisotropy, and the exponent  $\mu$  is assumed to be independent of  $\phi$ . Notice that inequality (2.26) holds at  $j \rightarrow 0$  for any anisotropy, regardless of mechanisms contributing to  $s_c$ . This indicates an instability of the glassy state at  $j \rightarrow 0$  with respect to any perturbations violating its isotropy. Using Eqs. (2.10) and (2.15), one can show that the angular dependence of  $\mu$  can be taken into account by the replacement

$$b \rightarrow b + \beta \ln(j_k / j) \quad (2.27)$$

in Eq. (2.17), which does not change qualitatively the above statement (here  $\beta = \partial \ln \mu / \partial \phi$ ). Such a situation arises due to a very strong nonlinearity of the function  $\exp[-(j_k / j)^\mu]$  about a point  $j = 0$ , where all derivatives of  $V(j)$  vanish. This can lead to the instability at  $j \rightarrow 0$ , even in the isotropic case, if one takes into account the Hall effect. Then  $\rho_{xx} = \rho_{yy} = \rho$ ,  $\rho_{xy} = -\rho_{yx} = \rho \tan \Omega$ , which gives  $g = 4 / \tan^2 \Omega$ , with  $\Omega$  the Hall angle.<sup>10</sup> However, in high- $T_c$  superconductors, the Hall effect is negligible, compared with the anisotropy [ $\tan \Omega \sim 10^{-2} - 10^{-3}$  at  $B < 10$  T (Ref. 25)].

A similar instability occurs in the case of power  $\mathbf{E}(\mathbf{j})$  of the form

$$E_\alpha = \rho_{\alpha\beta} j_\beta (j / j_k)^m \quad (2.28)$$

with angular dependent  $j_k$  and  $m$ . If  $m = \text{const}$ , one has  $s(j) = m$ , and Eq. (2.16) becomes

$$m > s_c(\phi). \quad (2.29)$$

If Eq. (2.29) holds, the instability arises at any  $j$ . That

feature of the power  $\mathbf{E}(\mathbf{j})$  with  $m = \text{const}$  does not already occur if one takes account of an angular dependence of  $m(\phi)$ . This can be done by substitution of Eq. (2.27) into Eq. (2.29) with  $\beta = \partial \ln m / \partial \phi$ . Then Eqs. (2.29), (2.16), and (2.17) reduce to a quadratic inequality for  $\ln(j_k/j)$ , which gives the instability domains as follows:

$$j < j_f^-, \quad j > j_f^+, \quad (2.30)$$

$$j_f^\pm = j_k \exp \frac{2(\rho_x \rho_y)^{1/2} [\text{sgn} \beta / \sqrt{g} \pm (1+m)^{1/2} / m]}{|\beta| (\rho_x \cos^2 \phi + \rho_y \sin^2 \phi)}. \quad (2.31)$$

Thus, the angular dependence of  $m$  leads to the splitting of the instability region (Fig. 3).

Both for  $V \sim \exp[-(j_k/j)^\mu]$  and  $V \sim j^m$ , the anisotropy can result in the instability at  $j \rightarrow 0$ , except the case  $m = 0$  which corresponds to the linear  $\mathbf{E}(\mathbf{j})$ . This fact could be interpreted as follows. One possibility is that highly anisotropic superconductors always have a linear part of  $\mathbf{E}(\mathbf{j})$  at small  $j$ , which provides a macroscopically stable resistive state. For example, it has been shown that the TAFF in highly anisotropic superconductors can result from thermally activated generation of dislocation pairs in the FLL.<sup>26</sup> Another variant which will be discussed below could be due to the appearance of nonuniform current structures.

The above results are summarized in Fig. 3, where the values  $j_{f1}$  and  $j_{f2}$  correspond to the flux-flow and flux-creep regimes, respectively. Here the existence of the domain  $0 < j < j_{f1}^-$ , as well as an instability at  $j > j_{f3}$  caused by a nonlinear flux flow<sup>18</sup> depends upon specific mechanisms of flux dynamics and external conditions (heat transfer to a coolant, etc.) By contrast, the existence of the region  $j_{f1}^+ < j < j_{f2}$  is only due to the anisotropy and the characteristic shape of nonlinear  $I-V$  curve of a superconductor (Fig. 1). Furthermore, we shall consider just that universal current region  $j_{f1}^+ < j < j_{f2}$ , and denote for simplicity  $j_{f1}^+$  as  $j_{f1}$ .

Let us evaluate the anisotropy level which is able to cause the instability. As follows from Fig. 3, the instability occurs provided  $j_{f1} < j_{f2}$ ; that is,  $j_{f1} < j_c$ , since  $j_{f2} \sim j_c$  at  $g \gg 1$  [see Eq. (2.25)]. The inequality  $j_{f1} < j_c$  reduces to  $g < g_c \sim j_c/j_1$  for the conventional flux-creep model and  $g < g_c \sim m$  for the power  $I-V$  curve. Taking typical for high- $T_c$  oxides values  $j_c/j_1 \sim 10-10^2$ , or  $m \sim 5-10^2$  (Refs. 16 and 17), one finds a similar estimation for both cases  $g_c \sim 10-10^2$ . As a result, the minimum values of  $|\rho_x - \rho_y| / (\rho_x + \rho_y)$  and  $b(\phi)$  prove to be of order  $4/\sqrt{g} \sim 0.1$  [see Eq. (2.17)]. Such an anisotropy in resis-

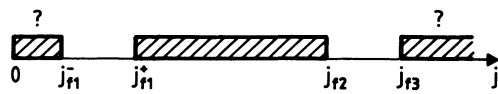


FIG. 3. Regions of the instability (hatched) along the  $j$  axis. The question marks indicate the domains whose existence depend on details of  $I(V)$  at low and high  $E$ .

tivity and critical current density is much smaller than that of high- $T_c$  superconductors for which  $\rho_a \sim 0.1\rho_c$  in the case of  $\text{YBa}_2\text{Cu}_3\text{O}_7$  and  $\rho_a \sim (10^{-4}-10^{-5})\rho_c$  for Bi-based compounds, and  $j_{c1}/j_{c2} \sim 10-10^2$ .<sup>27-31</sup> Here the indexes  $a$  and  $c$  correspond to the crystallographic axes of high- $T_c$  oxides, and  $j_{c1}$  and  $j_{c2}$  are critical current densities parallel and perpendicular to the  $ab$  plane. Therefore, the electromagnetic instability can occur at quite moderate anisotropy which can easily be realized in high- $T_c$  oxides as well as in other layered and quasi-1D superconductors.

#### D. Stability diagram

In this section we consider the dependence of the instability on current direction. Because of the invariance of  $\mathbf{E}(\mathbf{j})$  under inversion, the parameter  $b(\phi) = \partial \ln j_k / \partial \phi$  vanishes at  $\phi = \pi n / 2$ ,  $n = 0, \pm 1, \pm 2$  [see Eq. (2.4)] and can be expanded into a Fourier series of the form

$$b(\phi) = \sum_n b_n \sin 2n\phi. \quad (2.32)$$

This results in a characteristic angular dependence of  $s_c(\phi)$  shown in Fig. 4, with the function  $s_c(\phi)$  tending to infinity at  $\phi = \pi n / 2$ , since  $b(\phi) = 0$  and  $g(\phi) = \infty$ . The divergence of  $s_c(\phi)$  at  $\phi = \pi n / 2$  in Eq. (2.16) implies that the uniform current is always stable if  $\mathbf{j} \parallel \mathbf{x}$ , or  $\mathbf{j} \parallel \mathbf{y}$ . The function  $s_c(\phi)$  attains a minimum at  $\phi_m$  obeying the equation  $\partial g / \partial \phi = 0$  which reduces to

$$(\rho_x \cos^2 \phi_m + \rho_y \sin^2 \phi_m) \frac{db}{d\phi} = (\rho_x - \rho_y) [b(\phi_m) \sin 2\phi_m + \cos 2\phi_m]. \quad (2.33)$$

This equation determines the direction of  $\mathbf{j}$  for which the instability occurs at minimum value of  $s(j)$ . For instance,  $\phi_m = \pi/4$  at  $b = 0$ , whereas at  $\rho_x = \rho_y$ , the angle  $\phi_m$  obeys  $db/d\phi_m = 0$  (we consider here only the first quadrant  $0 < \phi < \pi/2$ ). Thus, the instability domain  $j_{f1}(\phi) < j < j_{f2}(\phi)$  essentially depends on the orientation of  $\mathbf{j}$ , reaching a maximum at  $\phi = \phi_m$  and vanishing in the vicinity of  $\phi \approx 0$  or  $\phi \approx \pi/2$ . For example, in the conventional flux-creep model, Eq. (2.23) yields, at  $\rho_x \gg \rho_y$ ,

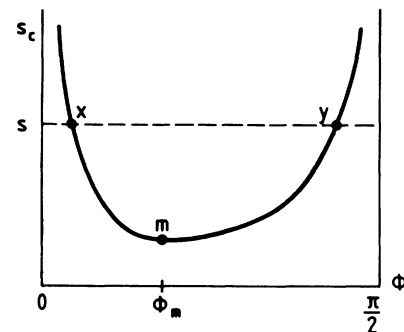


FIG. 4. The dependence of  $s_c$  on  $\phi$ . The intersections of  $s_c(\phi)$  with the dashed line  $s_c = s$  determine the instability region  $\phi_x < \phi < \phi_y$ .

$$j_{f1}(\phi) = \frac{\sqrt{6}(\rho_y/\rho_x)^{1/4}j_1(\phi)}{|\cos\phi[\sin\phi - b(\phi)\cos\phi]|^{1/2}}. \quad (2.34)$$

The angular dependence of  $j_{f1}(\phi)$  reveals sharp peaks at  $\phi \approx 0$  and  $\pi/2$  with a pronounced minimum at  $\phi = \phi_m$ . This means that uniform current is stable if it flows nearly parallel to the symmetry axes; that is, the angle of  $j$  with the  $x$  or  $y$  axes is smaller than the critical value  $\phi_c$  determined by the condition  $j_{f1}(\phi_c) \approx j_c(\phi_c)$ , which gives  $\phi_c \sim (j_1\rho_y/j_c\rho_x)^{1/2}$ . At  $\rho_x \gg \rho_y$ , the value  $j_{f1}(\phi)$  proves to be much less than  $j_c$ , except for narrow vicinities of the angles  $\phi \approx \pi n/2$ . A qualitative dependence of  $j_{f1}(\phi)$  is shown in Fig. 5.

Now we turn to the instability criterion (2.16) and examine its dependence on current direction by using a graphic analysis shown in Fig. 6. Here three characteristic dependences of  $s(j)$  at  $j < j_c$ , matching the standard flux-creep model [Fig. 6(a)], vortex glass [Fig. 6(b)], and power  $I$ - $V$  curve [Fig. 6(c)] are presented. The asymptotes of  $s(j)$  at  $j - j_c \gg j_1$  in all three cases correspond to the flux-flow regime for which  $s(j) = j_c/(j - j_c)$ . The dashed line in Fig. 6 has the ordinate  $s_c(\phi)$ , and its intersections with  $s(j)$  give the values  $j_{f1,2}(\phi)$ .

Let us now consider what happens when changing the current direction if the vector  $j$  has initially been directed along the  $x$  axis. According to Fig. 4, the function  $s_c(\phi)$  decreases with  $\phi$ , which leads to the lowering of the dashed line in Fig. 6 as  $\phi$  increases from 0 to  $\phi_m$ . The uniform state is stable provided that the dashed line lies above  $s(j)$ . At small  $\phi$ , such a situation does occur for Figs. 6(a) and 6(c), whereas Fig. 6(b) corresponds to the instability at low  $j$  for any nonzero misalignment of  $j$  and  $x$ . In Figs. 6(a) and 6(c), the instability domain  $j_{f1}(\phi) < j < j_{f2}(\phi)$  arises if the angle  $\phi$  exceeds the critical value  $\phi_{xc}$  determined by  $s_{\max} = s_c(\phi_{xc})$ , with  $s_{\max}$  the maximum of  $s(j)$ . For Fig. 6(a), one has  $s_{\max} \approx j_c/j_1$ , which follows from both asymptotes of  $s(j)$  at  $j - j_c \gg j_1$  and  $j_c - j \gg j_1$  taken in the crossover region  $|j_c - j| \sim j_1$ . Furthermore, we get  $s_{\max} = m$  for curve 1 in Fig. 6(c), whereas the value of  $s_{\max}$  for curve 2 depends on details of the crossover between the flux-flow and flux-creep regimes. For curve 1, the passing through  $\phi = \phi_{xc}$  results in a jumpwise appearance of a finite instability domain

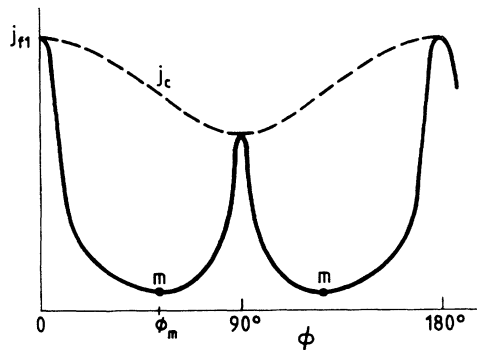


FIG. 5. The angular dependence of  $j_{f1}(\phi)$ . The dashed curve shows  $j_c(\phi)$ .

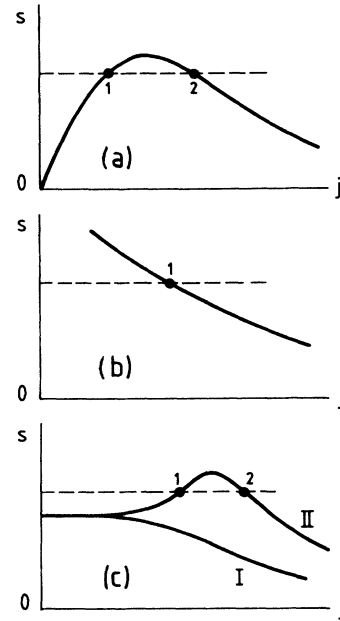


FIG. 6. Characteristic dependences of  $s(j)$  for (a) conventional flux-creep model, (b) vortex glass, and (c) power  $I$ - $V$  curve at  $j < j_c$ . The dashed lines correspond to  $s = s_c(\phi)$  at fixed  $\phi$ .

$0 < j < j_{f1}$  at low  $j$ . If  $s(j)$  has a maximum at nonzero  $j$ , the instability domain arises at nonzero  $j$  as well, its width growing continuously with  $\phi$  as follows:  $j_{f2}(\phi) - j_{f1}(\phi) \propto (\phi - \phi_{xc})^{1/2}$  at  $\phi - \phi_{xc} \ll \phi_{xc}$ .

It is also convenient to present these results in somewhat different form, by examining stable and unstable directions in the  $xy$  plane. Such an angular stability diagram is shown in Fig. 7, where there are several characteristic sectors marked as stable, metastable, and unstable. The stable sectors  $0 < \phi < \phi_{xc}$  and  $\phi_{yc} < \phi < \pi/2$  correspond to the absolute stability of uniform current state to small electromagnetic perturbations at all  $j$ . At  $\phi_{xc} < \phi < \phi_{yc}$  the uniform current turns out to be unstable within the domain  $j_{f1}(\phi) < j < j_{f2}(\phi)$  and metastable at

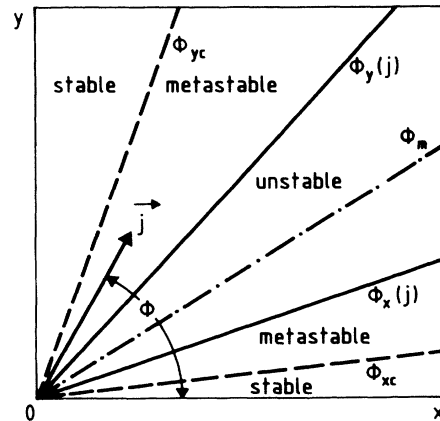


FIG. 7. Angular stability diagram. The angles  $\phi_x$ ,  $\phi_y$ ,  $\phi_{xc}$ ,  $\phi_{yc}$ , and  $\phi_m$  are determined by the graphic solution of  $s(j) = s_c(\phi)$  shown in Fig. 4.

$j_{f1}(\phi_m) < j < j_{f1}(\phi)$  or  $j_{f2}(\phi) < j < j_{f2}(\phi_m)$ .

Let us consider, for example, how the instability arises when increasing  $j$  at fixed  $\phi$  for the case shown in Fig. 6(a). At  $j < j_{f1}(\phi_m)$  [ $s(j) < s_c(\phi_m)$ ], the instability criterion (2.16) does not hold at any  $\phi$ , which implies that both metastable and unstable sectors in Fig. 7 disappear. At  $j > j_{f1}(\phi_m)$  the unstable sector arises in the vicinity of  $\phi = \phi_m$  with the angular width  $\phi_y - \phi_x \propto [j - j_{f1}(\phi_m)]^{1/2}$  increasing with  $j$  (see Figs. 4 and 7). At  $\phi_{xc} < \phi < \phi_x(j)$  or  $\phi_y(j) < \phi < \phi_{yc}$  the uniform current flow is metastable with respect to finite-amplitude perturbations  $\delta j$ , since an increase of  $j$  results in the narrowing of the metastable sectors. At  $j > j_{f1}(\phi)$ , the vector  $\mathbf{j}$  gets into the unstable sector, and at  $j = j_m$  the metastable sectors disappear [ $s(j_m) = s_{\max}$ ]. The further increase of  $j$  results in a recovery of the metastability of the current state at  $j = j_{f2}(\phi)$  and its absolute stability at  $j > j_{f2}(\phi_m)$ .

Thus, the instability at fixed  $\phi$  occurs when the stability boundaries  $\phi = \phi_{x,y}(j)$  cross the vector  $\mathbf{j}$  as the modulus  $j$  changes. These boundaries separating unstable and metastable states can be treated as spinodals in the angular space by analogy with the thermodynamic spinodals at first-order phase transitions. Besides, the physical mechanism of both the electromagnetic instability and the classic spinodal decomposition is due to that the corresponding diffusion coefficient vanishes. For example, the spinodal decomposition of alloys is due to a negative diffusivity of a component, which is accompanied by the appearance of concentration structures.<sup>32</sup> Likewise, the above instability of resistive states is due to the negative magnetic diffusivity  $D_2$  along the  $\zeta$  axis, which also leads to a spontaneous growth of inhomogeneities in vortex density and appearance of magnetic flux structures. Therefore, the electromagnetic instability in anisotropic superconductors could be interpreted in terms of a kinetic phase transition resulting in the magnetic spinodal decomposition of the uniform current state. That analogy will be discussed below in more detail.

### E. Short-wave spectrum

The above analysis based only on the macroscopic electrodynamics and symmetry properties of  $\mathbf{E}(\mathbf{j})$ , gives a diffusionlike spectrum (2.5) for which the increment  $\lambda(\mathbf{k})$  monotonously decreases or increases with  $k$ , depending on whether the criterion (2.16) holds, or not. Above the threshold [ $s > s_c$ ,  $\text{Re}f(\mathbf{n}) < 0$ ] an explosive instability arises since the growth rate of electromagnetic perturbations approaches infinity [ $\lambda(\mathbf{k}) \rightarrow \infty$ ] at  $k \rightarrow \infty$ . However, the large  $k$  correspond to short wavelengths comparable with microscopic lengths over which vortex structures are wittingly stable and  $\lambda(\mathbf{k}) < 0$ . This implies that the increment  $\lambda(\mathbf{k})$  actually passes through a maximum at some  $k = k_m$  as it is shown in Fig. 2. The drop of  $\lambda(\mathbf{k})$  at large  $k$  is due to additional mechanisms suppressing the short-wave instability which is beyond the scope of the macroscopic approach. We briefly discuss these mechanisms here since they become important for the description of nonlinear current structures arising at  $s > s_c$ .

Generally, the modification of the spectrum  $\lambda(\mathbf{k})$  at large  $k$  is due to a nonlocality of  $I$ - $V$  curves for short-wave perturbations  $\delta \mathbf{E}(\mathbf{r}, t)$  which are determined not only by the local value  $\delta j(\mathbf{r}, t)$ , but values  $\delta j(\mathbf{r}', t')$  within some domain  $|\mathbf{r} - \mathbf{r}'| k_m < 1$  as well; that is,

$$dE_\alpha = \int R_{\alpha\beta} \left[ \frac{|\mathbf{r} - \mathbf{r}'|}{l}, \frac{|t - t'|}{\tau} \right] \delta j_\beta(\mathbf{r}', t') d^2 r dt',$$

where the tensor  $R_{\alpha\beta}(\mathbf{r}, t)$  becomes a kernel varying over characteristic length  $l$  and time  $\tau$ . In the Fourier representation this leads to a dependence of  $R_{\alpha\beta}$  on  $\mathbf{k}$  at large  $k$ , therefore the results of the previous sections are valid at  $k \ll k_m$ . Otherwise the time and space dispersion of  $R_{\alpha\beta}$  turn out to be important and the local  $R_{\alpha\beta}$  in all formulas obtained above should be replaced by the values  $R_{\alpha\beta}(\mathbf{k}, \omega)$  which depend on  $\mathbf{k}$  and  $\omega$ .

There are both macroscopic and microscopic mechanisms leading to the space and time dispersion of  $R_{\alpha\beta}(\mathbf{k}, \lambda)$ , for example, the coupling of the electromagnetic perturbations with the diffusion of heat or non-equilibrium quasiparticles accompanying the vortex motion. For a film of thickness  $d$ , the characteristic thermal time  $t_0$  and length  $l$  are given by  $t_0 \sim C/h_0 d$  and  $l \sim (d\kappa/h_0)^{1/2}$ , with  $C$  the heat capacity,  $\kappa$  the thermal conductivity, and  $h_0$  the heat transfer coefficient,<sup>22</sup> the dispersion of  $R_{\alpha\beta}$  manifesting itself at  $\lambda t_0 > 1$  and  $kl > 1$ . The electron diffusion time and length are as follows:  $t_0 \sim \tau_{\text{ph}}$ ,  $l \sim (D_e \tau_{\text{ph}} k_B T / \Delta)^{1/2}$  with  $\tau_{\text{ph}}$  the electron-phonon inelastic scattering time,  $D_e$  the electron diffusivity, and  $\Delta$  the superconducting energy gap.<sup>18,33</sup> The dispersion of  $R_{\alpha\beta}(\mathbf{k})$  can also be due to hydrodynamic modes of the mixed state,<sup>34</sup> dispersion of elastic moduli of FLL,<sup>35</sup> pinning (if the wavelength  $2\pi/k$  becomes comparable with the pinning correlation length),<sup>18</sup> etc. Another mechanism can be due to a granularity typical for both ceramic and single-crystalline high- $T_c$  oxides<sup>36-39</sup> since the existence of weakly coupled grains of size  $l$  leads to the dispersion of  $R_{\alpha\beta}(\mathbf{k})$  at  $kl > 1$ .

Near the instability threshold  $s = s_c$ , the characteristic values of  $k$  are much smaller than  $l$  (see below), therefore  $R_{\alpha\beta}(\mathbf{k})$  can be expanded up to second-order terms in  $\mathbf{k}$  as follows:

$$R_{\alpha\beta}(k) = R_{\alpha\beta} + P_{\alpha\beta\gamma\delta} k_\gamma k_\delta, \quad (2.35)$$

where  $R_{\alpha\beta}$  corresponds to  $k = 0$ ,  $P_{\alpha\beta\gamma\delta} = \frac{1}{2} \partial^2 R_{\alpha\beta}(\mathbf{k}) / \partial k_\gamma \partial k_\delta |_{\mathbf{k}=0}$ , and terms linear in  $\mathbf{k}$  vanish due to the invariance under inversion. At  $s \rightarrow s_c$ , the non-local corrections are essential only for the principal value  $R_2(j)$  vanishing at  $s = s_c$ , whereas for the finite  $R_1$  they can be neglected. In this case the long-wavelength spectrum  $\lambda(\mathbf{k})$  becomes

$$\lambda(\mathbf{k}) = -\mu_0^{-1} R_1 (k_\xi^2 - \epsilon k_\eta^2 + l^2 k_\eta^4), \quad (2.36)$$

where  $\epsilon = -R_2/R_1 \sim (s - s_c)/s_c \ll 1$  is a bifurcation dimensionless parameter, and  $k_\xi$  and  $k_\eta$  are the components of  $\mathbf{k}$  along the principal axes of  $R_{\alpha\beta}$ . The last term in Eq. (2.36) coming from the nonlocality results in a maximum in  $\lambda(\mathbf{k})$  at  $k_\xi = 0$ ,  $l k_\eta = (\epsilon/2)^{1/2}$  at  $\epsilon > 0$ . Here

$$l^2 = |P_{\alpha\beta\gamma\delta} n_\alpha n_\beta n_\gamma n_\delta| / R_1, \quad (2.37)$$

where  $P_{\alpha\beta\gamma\delta}$  is determined by the above-discussed mechanisms of dispersion, and the unit vector  $\mathbf{n}$  fixed by Eqs. (2.11) and (2.19) corresponds to the critical mode with  $k_\xi = 0$  (Fig. 2). Notice that, at  $\epsilon \ll 1$ , one can neglect small terms proportional to  $k_\eta^2 k_\xi^2$  and  $k_\xi^4$  in  $\lambda(\mathbf{k})$ , therefore the long-wavelength spectrum depends only on one length  $l$  given by Eq. (2.37). In the coordinate representation, the spectrum (2.36) corresponds to the following equation for  $\delta H$ :

$$\mu \partial_t \delta H = (\partial_{\xi\xi}^2 - \epsilon \partial_{\eta\eta} - l^2 \partial_{\eta\eta\eta\eta}) \delta H \quad (2.38)$$

with  $\mu = \mu_0 / R_1$ .

### III. NONLINEAR CURRENT PATTERNS

#### A. Qualitative analysis

So far we have considered only the linear stability of the uniform resistive state to small perturbations  $\delta H(\mathbf{r}, t)$ . Now we examine nonlinear current structures caused by the instability at  $s > s_c$ . As seen from Fig. 2, the instability induces transversal components  $\delta \mathbf{j}(\mathbf{r}, t)$  to the initial  $\mathbf{j}$ , which is just a local turn of  $\mathbf{j}$  toward a new direction corresponding to a lower resistance in the  $xy$  plane. This leads to current patterns which depend on the sample geometry since the uniform turn of  $\mathbf{j}$  is usually incompatible with the boundary conditions which ensure zero normal components of  $\mathbf{j}(\mathbf{r})$  at the lateral surface. Two characteristic examples are shown in Figs. 8 and 9. In the first case (Fig. 8), a thin-film strip carries a transport current flowing along the symmetry plane  $xy$ . Above the threshold  $s > s_c$  the uniform flow becomes unstable with respect to the local turn of  $\mathbf{j}$ . This leads to the appearance of a nonuniform current state due to a partial closure of current lines caused by the effect of the strip edges. In the second case (Fig. 9), a superconducting slab is in a slowly increasing magnetic field  $\mathbf{H}_e(t)$ . Here the distribution of induced electric fields and closed screening currents are determined by the sweep rate  $\dot{H}_e = dH_e/dt$  and the orientation of  $\mathbf{H}_e$  with respect to the sample sides or the symmetry axes, at low enough  $\dot{H}_e$  the current flow being laminar. Above the critical value of  $\dot{H}_e$  the local stability criterion  $s(j(\mathbf{r})) < s_c(\phi(\mathbf{r}))$  violates in some regions of the sample, which results in the appearance of additional components  $\delta \mathbf{j}(\mathbf{r})$  to the initial  $\mathbf{j}(\mathbf{r})$ . The char-

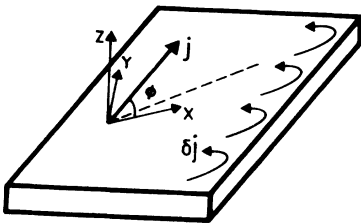


FIG. 8. Formation of macroscopic vortices in a thin-film strip due to the local turn of  $\mathbf{j}$  toward a lower-resistance direction (dashed).

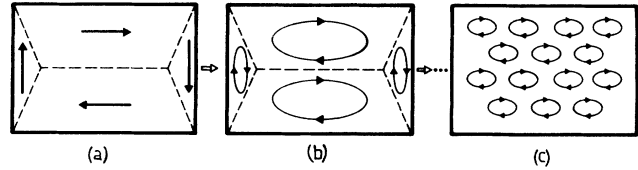


FIG. 9. Successive stages of the current fragmentation in a slab. The singular lines (dashed) play the role of self-induced weak lines, as explained in the text.

acter of the current patterns depends on the relation between  $\delta \mathbf{j}$  and  $\mathbf{j}$ . For instance, at  $\delta \mathbf{j} \ll \mathbf{j}$ , there arise only weak modulations of the initial current distribution, whereas at  $\delta \mathbf{j} > \mathbf{j}$  the instability results in a partial closure of current lines and appearance of anisotropic current loops, which can be treated as a macroscopic-vortex structure for which  $\text{curl} \delta \mathbf{j} \neq 0$ .<sup>10</sup> In general, this changes both the value and the orientation of the magnetic moment  $\mathbf{M}$  with respect to the symmetry axes and the sample sides.

As an illustration, Fig. 9 shows the formation of the macroscopic-vortex structure in the slab in the case  $\mathbf{H}_e \parallel \mathbf{z}$ . For simplicity, we restrict ourselves to the strong anisotropy limit allowing a clear physical interpretation in terms of the anisotropic Bean model. In this case the extended Bean model<sup>11</sup> predicts the current flow along a rectangular path which contains the singular lines, where the current sharply changes the direction by  $90^\circ$ . The latter is due to the ignoring of the resistive part of  $\mathbf{j}(\mathbf{E})$ , since within the framework of the critical-state concept the real  $I$ - $V$  curve is replaced by the stepwise function  $I = I_c \text{sgn} V$ . Since, however, some electric field always exists due to the flux creep, this would lead to discontinuities of tangential components  $\mathbf{E}_t$  at the singular lines, in contradiction to electrodynamics which requires the continuity of  $\mathbf{E}_t$  at any interface. Actually, these discontinuities disappear when taking into account the flux diffusion in terms of the Maxwell equations and more adequate  $I$ - $V$  curve similar to that shown in Fig. 1. This results in the rounding of the current lines in the corners of the slab over macroscopic scales determined by the shape of  $I(V)$  and the aspect ratio. Unlike the isotropic case, where this effect leads only to a correction to  $M$ , the bend of current lines in the anisotropic case can cause the instability due to the strong angular dependence of  $j_{f1}(\phi)$  shown in Fig. 5.

Indeed, in the vicinity of the singular lines there exists a macroscopic layer, where current lines sharply change the direction and there is a large misalignment between  $\mathbf{j}$  and the symmetry axes. As follows from Fig. 5, the latter leads to a considerable drop of  $j_{f1}(\phi)$  as compared with  $j_c$ , therefore the maximum nondissipative current density through the singular lines is limited by the small value  $j_{f1}(\phi_m) \ll j_c$ . This enables one to treat the singular lines as peculiar self-induced weak links whose form and distribution are determined in a self-consistent manner by the overall current configuration. As a result, the currents with  $j \sim j_c$  flowing along the  $x$  and  $y$  axes cannot pass

completely through the singular lines, which results in the splitting of the initial current loop into four smaller ones, as is shown in Fig. 9(b). Then, one can again apply the Bean model to each of the domains being within the dashed contours and get new singular lines which provide the closure of the magnetization currents and, as a consequence, the further division of current loops. The process of successive fragmentation of macroscopic current loops into smaller ones goes on as long as the sizes of the loops become comparable with the above-discussed microscopic scale  $l$  over which the vortex structure is stable. Thus, for strong anisotropy [ $j_{f1}(\phi_m) \ll j_c(\phi)$ ] the current patterns at  $s > s_c$  consist of an array of magnetic macroscopic vortices of size  $\sim l$  with closed screening current densities ( $\sim j_c$ ) well above the mean macroscopic value  $\sim j_{f1}(\phi_m)$ .

Such a structure could be outlined as follows. In the high anisotropy limit  $s(j) \gg s_c(\phi)$ , the angular width  $\phi_c$  of the stability sectors in Fig. 7 becomes very narrow [as follows from Eqs. (2.22) and (2.23),  $\rho_c \sim (\rho_y j_1 / \rho_x j_c)^{1/2}$  at  $\rho_x \gg \rho_y$ ]. This implies that stable uniform currents can flow nearly parallel to the symmetry axis, which impose strong restrictions on the form of current patterns. For instance, in a thin-film strip shown in Fig. 10, the current structure could consist of an array of resistive current channels, each of them being nearly parallel to either the  $x$  or the  $y$  axes. However, characteristic width of the channels as well as the spacing between them cannot considerably exceed  $l$ , otherwise the existence of macroscopic low-resistivity regions between the channels is incompatible with  $\text{curl} \mathbf{E} = 0$  (the regions electrically short the channels). Likewise, one can estimate a width of the channels by considering an intersection of two channels shown in Fig. 10. If the width of the channels is much larger than  $l$ , they can be considered macroscopically, thereby the region where the current lines sharply change the direction by  $90^\circ$  over the length  $\sim l$  turns into a discontinuity of the tangential component  $E_t$ , which is again incompatible with  $\text{curl} \mathbf{E} = 0$ . Therefore, at  $s \gg s_c$ , sizes of the macroscopic vortices turn out to be of order  $l$ , whence it follows that a description of such a state can actually be done only within the framework of microscopic models of the mixed state. In the case of a moderate anisotropy, sizes of the macroscopic vortices can be much larger than  $l$ . This requires an analysis of macroscopic nonlinear current structures which will be discussed later on.

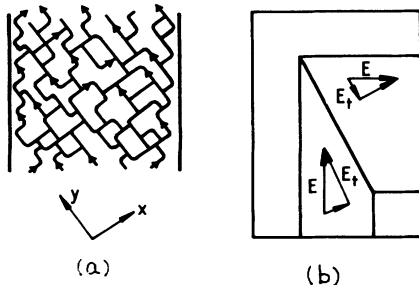


FIG. 10. Possible pattern of current channels in the high anisotropy limit (a). A fragment of the channel intersection (b).

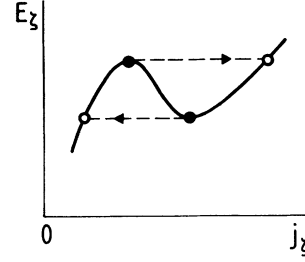


FIG. 11.  $I$ - $V$  curve along the  $\zeta$  axis at fixed  $j_\eta$ .

Notice that the appearance of the macroscopic-vortex structure can be accompanied by a hysteresis, which follows from the form of the  $I$ - $V$  curve (2.3) along the  $\zeta$  axis at fixed  $j_\eta$ . Shown in Fig. 11, the  $N$ -shaped dependence  $E_\zeta(j_\eta)$  reflects the main qualitative features of the angular diagram in Fig. 7 since the change of  $j_\zeta$  at fixed  $j_\eta$  is equivalent to the change of  $\phi$  in Fig. 7. For instance, the solid points, where  $\partial E_\zeta / \partial j_\zeta = 0$ , correspond to  $\phi = \phi_x$  and  $\phi = \phi_y$  in Fig. 7. Furthermore, the part of  $E_\zeta(j_\eta)$  with a negative slope matches the unstable sector in Fig. 7, whereas the parts of  $E_\zeta(j_\zeta)$  with positive slopes, being between the solid and open points, correspond to the metastable sectors. As seen from Fig. 11, slow variations of  $E_\zeta$  can result in hysteretic jumpwise changes of  $j_\zeta$  and, therefore, the current direction. Such turns of  $\mathbf{j}$  could also be due to strong perturbations which cause transitions of the representing point between stable branches of the function  $E_\zeta(j_\zeta)$ . These features are manifestations of a first-order kinetic phase transition which will be considered in the next section. As mentioned in the Introduction, the transition may be considered as an analog of the field-induced orientational instability in liquid crystals. In particular, for a nematic being between two parallel glassy plates, longitudinal electric or magnetic fields can cause a jumpwise turn of the director which has initially been oriented perpendicular to the plates by surface effects (the so-called Frederiks transition).<sup>15</sup>

### B. Kinetic phase transition

In this section we consider low-amplitude ( $\delta \mathbf{j} \ll \mathbf{j}$ ) structures at the instability threshold in the simplest case of the 2D instability in an infinite thin-film strip connected to a dc power supply. The condition of the fixed current  $I$  reads

$$\int \delta \mathbf{j}(\mathbf{r}) d^2 r = 0 \quad (3.1)$$

with the integral taken over the cross section. The results of the 2D analysis can be applied to the 3D case as well, provided that the current flows parallel to the symmetry plane  $xy$ , and  $\mathbf{B} \parallel z$ . In order to describe the low-amplitude current structures at  $s - s_c \ll s_c$ , one should take into account second-order nonlinear terms in Eq. (2.38), which gives

$$\begin{aligned} \mu_0 \partial_t \delta H = & R_1 \partial_{\zeta^2} \delta H + (R_2 + N \partial_\eta \delta H) \partial_{\eta \eta} \delta H \\ & - l^2 R_1 \partial_{\eta \eta \eta \eta} \delta H . \end{aligned} \quad (3.2)$$

This equation is an expansion of the Maxwell equations in current perturbations  $\delta j$ , where we keep only the nonlinear contribution to the critical mode with  $\mathbf{k} = k\mathbf{n}$ , which results in the instability at  $s = s_c$ ; the rest terms are of the next order in  $\epsilon$ . It is convenient to rewrite Eq. (3.2) in terms of the dimensionless field  $h = \delta H/H_1$ , with  $H_1 = 2R_1/N$  as follows:

$$\mu \partial_t h = \partial_{\zeta\zeta} h - \epsilon \partial_{\eta\eta} h + 2\partial_{\eta} h \partial_{\eta\eta} h - l^2 \partial_{\eta\eta\eta} h, \quad (3.3)$$

where  $\mu = \mu_0/R_1$ , and  $\epsilon = -R_2/R_1 \sim (s - s_c)/s_c \ll 1$  is the dimensionless control or bifurcation parameter (explicit formulas for  $\epsilon$  and  $N$  are given in Appendix B). Notice that the length  $l$  can be excluded from Eq. (3.3) by the rescaling of  $h$ ,  $\zeta$ , and  $\eta$ , therefore Eq. (3.3) describes a universal behavior near the bifurcation point  $\epsilon = 0$ , regardless of specific shape of  $\mathbf{E}(\mathbf{j})$  and origin of the dispersion of  $R_{\alpha\beta}(\mathbf{k})$ . Equation (3.3) can be obtained by varying a functional  $Q\{h\}$  as follows:

$$\mu \partial_t h = -\frac{\delta Q}{\delta h}, \quad (3.4)$$

$$Q = \int \left[ \frac{1}{2} (\partial_{\zeta} h)^2 - \frac{\epsilon}{2} (\partial_{\eta} h)^2 + \frac{1}{3} (\partial_{\eta} h)^3 + \frac{l^2}{2} (\partial_{\eta\eta} h)^2 \right] d\eta d\zeta. \quad (3.5)$$

As seen from Eqs. (3.4) and (3.5), the dynamics of  $h(\mathbf{r}, t)$  has a relaxation character, i.e., Eq. (3.3) has only stationary or monotonously changing with  $t$  dynamic solutions. Besides, any evolution of the dimensionless current perturbations  $\delta j_{\eta} = -\partial_{\zeta} h$  and  $\delta j_{\zeta} = \partial_{\eta} h$  is to result in a minimum of  $Q\{h\}$ . This situation is analogous to that of equilibrium phase transitions, with  $\delta j_{\zeta}$  and  $Q$  playing the roles of an order parameter and kinetic potential, respectively. The dependence of  $Q$  on  $\delta j_{\zeta}$  shown in Fig. 12 is typical for the first-order phase transitions.

Due to a finite potential barrier in  $Q\{\delta j_{\zeta}\}$  at  $\epsilon < 0$ , the metastable uniform stationary state  $\delta j_{\zeta} = \delta j_{\eta} = 0$  can be destroyed by external noise, thermal fluctuations, etc. The transition results from a nucleation and subsequent growth of critical nuclei of a new "phase" with  $\delta j_{\eta} \neq 0$ . The critical nucleus is described by a stationary unstable solution of Eq. (3.3) which corresponds to a saddle point of  $Q\{h\}$ . To analyze the current distribution in the nucleus, we consider first a 1D stationary solution of Eq. (3.3) which depends only on  $\eta$ , with  $\partial_{\eta} h = 0$  at  $\eta = \pm\infty$ .

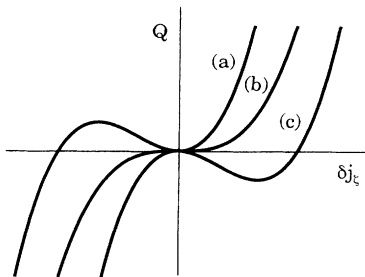


FIG. 12. Kinetic potential  $Q$  vs  $\delta j_{\zeta}$  in the case of (a)  $s < s_c$ , (b)  $s = s_c$ , and (c)  $s > s_c$ .

As shown in Appendix C, such a solution exists only at  $\epsilon < 0$  and has the following form:

$$\delta j_{\zeta}(\eta) = \partial_{\eta} h(\eta) = \frac{3\epsilon}{2 \cosh^2(\eta/2L_{\eta})} \quad (3.6)$$

with the correlation length  $L_{\eta} = 1/|\epsilon|^{1/2}$ . Formula (3.6) describes a ribbon of width  $L_{\eta}$ , where the vector  $\mathbf{j}$  is slightly inclined with respect to the initial current flow due to the nonzero component  $\delta j_{\zeta}(\eta)$ . Since, however, the uniform turn of  $\mathbf{j}$  in the ribbon is incompatible with the boundary conditions, one has to take into account the term  $\partial_{\zeta\zeta} h$  in Eq. (3.3) which leads to the closure of the current lines. As a result, the 1D distribution (3.6) turns into a chain of macroscopic vortices of length  $L_{\zeta}$  along the  $\zeta$  axis. The value  $L_{\zeta}$  can be estimated from Eq. (3.5) since the potential  $Q\{h\}$  is to be minimum for any steady state  $h(\zeta, \eta)$ . By inserting Eq. (3.6) into Eq. (3.5), one gets that  $Q \sim \epsilon^{5/2} L_{\zeta}$ , where  $L_{\zeta}$  is the length of the nucleus along the  $\zeta$  axis. The minimum of  $Q$  corresponds to the value of  $L_{\zeta}$  at which the term  $\epsilon(\partial_{\eta} h)^2$  in Eq. (3.5) becomes of order  $(\partial_{\zeta} h)^2$ , hence  $h^2/L_{\zeta}^2 \sim \epsilon h^2/L_{\eta}^2$  and  $L_{\zeta} = 1/|\epsilon| \gg L_{\eta}$ . Such a critical nucleus is a highly anisotropic macroscopic vortex, with the length  $L_{\zeta}$  along the  $\zeta$  considerably exceeding the length  $L_{\eta}$  along the  $\eta$  axis. The dynamics of the thermally activated generation of the critical nuclei can be described in a standard way<sup>40,41</sup> by adding to the right side of Eq. (3.2) a random "force"  $\xi(\mathbf{r}, t)$  with the correlation function

$$\langle \xi(\mathbf{r}, t) \xi(\mathbf{r}', t') \rangle = 2k_B T \Gamma \delta(\mathbf{r} - \mathbf{r}') \delta(t - t'), \quad (3.7)$$

where  $\Gamma = \mu_0(R_1 \partial_{\zeta\zeta} + R_2 \partial_{\eta\eta})$ .

At  $\epsilon > 0$ , the uniform state  $\delta j_{\zeta} = \delta j_{\eta} = 0$  turns out to be unstable due to the magnetic spinodal decomposition caused by the negative principal value  $R_2$ . The passing through  $\epsilon = 0$  leads to the growth of current structures whose initial dynamics is described by the universal equation (3.3). However, the final stage of the growth can be described only by the full Maxwell equations in which the space dispersion of  $R_{\alpha\beta}(\mathbf{k})$  should be taken into account. This is due to the amplitude  $\delta j(\mathbf{r})$  of the stationary structures not being small and depends on the shape of  $\mathbf{E}(\mathbf{j})$  and specific mechanisms of the nonlocality. For instance, in Appendix C, it is shown that there are no stationary low-amplitude 1D solutions of Eq. (3.3) obeying Eq. (3.1).

Therefore, the electromagnetic instability can be formulated as a first-order kinetic phase transition described by the universal equation (3.3) similar to those of the relaxation dynamics of equilibrium phase transitions.<sup>40,41</sup> The meaning of the kinetic transition can be clarified by the angular stability diagram in Fig. 7, where one can formally identify two states for which the vectors  $\mathbf{j}$  are within the stable sectors to the  $x$  and  $y$  phases, respectively. These phases are separated in the angular space by metastable and unstable regions. Let  $\mathbf{j}$  be initially fixed within the metastable sector of the  $y$  phase. Since the unstable sector expands as the parameter  $s(j)$  increases, the  $y$  phase becomes unstable when the spinodal  $\phi_y(j)$  passes through the vector  $\mathbf{j}$ . This transition is just a turn of  $\mathbf{j}$  such that the vector  $\mathbf{j}$  gets into the sector of metastability

of the  $x$  phase. The analogous orientational transition from the  $x$  phase to the  $y$  phase occurs if the vector  $\mathbf{j}$  has initially been within the metastable  $x$  sector.

The  $x \rightarrow y$  transition occurs at  $0 < \phi < \phi_t$ , whereas the  $y \rightarrow x$  transition arises at  $\phi_t < \phi < \pi/2$ . Here  $\phi_t$  is the angle at which the coefficient  $N(\phi) = \frac{1}{2} \partial^2 E_\xi / \partial j_\xi^2$  in Eq. (3.2) changes the sign, and  $E_\xi(j_\xi)$  has a bending point (Fig. 11). As shown in Appendix B,  $\phi_t$  obeys the equation

$$\left[ 1 + \frac{\partial \psi}{\partial \phi} \right] \cos(\phi + \psi) \frac{\partial s}{\partial j} + \left[ \frac{1}{j} \sin(\psi + \phi) + \cos(\phi + \psi) \frac{\partial \psi}{\partial j} \right] \frac{\partial s_c}{\partial \phi} = 0 \quad (3.8)$$

with  $s(j)$ ,  $s_c(\phi)$ , and  $\psi(j, \phi)$  given by Eqs. (2.16)–(2.19); in the final formula (3.8) one should put  $j = j_{f1}(\phi)$ . If the first term in Eq. (3.8) is small as compared with the second one, the angle  $\phi_t$  approaches the angle  $\phi_m$  at which  $\partial s_c / \partial \phi = 0$ . In the vicinity of  $\phi = \phi_t$  and  $s \rightarrow s_c$ , where the quadratic term in Eq. (3.2) is small, one has to take into account other nonlinear terms proportional to  $\partial_\eta H \partial_\xi \eta^2 H$ ,  $\partial_\xi H \partial_\eta \eta^2 H$  and  $(\partial_\eta H)^2 \partial_\eta \eta H$ . At  $\phi \rightarrow \phi_t$  and  $s \rightarrow s_c$ , the transition becomes nearly of the second order, with  $\phi_t$  playing the role of a “critical” point in the angular space. Since, however, the uniform turn of the averaged current density  $\langle \mathbf{j} \rangle$  in the strip is impossible because of the boundary conditions, the vector  $\langle \mathbf{j} \rangle$  remains within the unstable sector of the angular diagram, where only uniform current structures can exist. Hence, it follows that the boundary conditions here play a very important role since just their effect leads to the stabilization of the nonuniform current state. By contrast, structures arising at classical spinodal decomposition are only transient stages upon transitions from unstable to stable phases.<sup>32</sup>

### C. Macroscopic-vortex structures

In an anisotropic medium, a nonuniform stationary current flow is generally vortical, which implies a partial closure of current lines and appearance of closed current loops. In this case the Maxwell equations  $\text{curl } \mathbf{E} = 0$  and  $\text{div } \mathbf{j} = 0$  have solutions with  $\text{curl } \mathbf{j} \neq 0$ , which follows already from the linear Eq. (2.13) describing a potential current flow ( $\partial_{\xi\xi} H + \partial_{\eta\eta} H = 0$ ) only for uniform currents ( $\partial H \propto \eta$ ). However, in the nonlinear case the anisotropy can also break the continuity of current flow, resulting in the appearance of singular interfaces at which jumps of tangential components  $\mathbf{j}_t$  occur. These features can be analyzed by using a transformation of the stationary Maxwell equations from the physical  $xy$  plane onto the so-called hodograph plane  $(j_x, j_y)$ . If one neglects the self-field effects, by assuming that  $E_\alpha(\mathbf{j}, \mathbf{H}) = E_\alpha(\mathbf{j}, \mathbf{H}_e)$  with  $\mathbf{H}_e$  the external magnetic field, the hodograph transformation reduces the nonlinear Maxwell equations to one linear equation. Such a procedure enables one to formulate a quasihydrodynamic approach for the description of nonlinear current flow and use some important results obtained for similar problems in aerodynamics,<sup>42</sup> theory of crystallization,<sup>44</sup> etc. In the case under con-

sideration, the hodograph transformation is as follows (details are given in Appendix D).

Let us introduce a function  $U(\mathbf{j})$  such that  $x = \partial U / \partial j_y$  and  $y = -\partial U / \partial j_x$ . Then the quantities  $j_x = j \cos \phi$ ,  $j_y = j \sin \phi$ , and  $U(j, \phi)$  are related to  $x$ ,  $y$ , and  $H$  as follows:

$$x = \sin \phi \frac{\partial U}{\partial j} + \frac{1}{j} \cos \phi \frac{\partial U}{\partial \phi}, \quad (3.9)$$

$$y = -\cos \phi \frac{\partial U}{\partial j} + \frac{1}{j} \sin \phi \frac{\partial U}{\partial \phi}, \quad (3.10)$$

$$H = U - j \frac{\partial U}{\partial j}. \quad (3.11)$$

In this case the nonlinear equation for  $H(x, y)$  reduces to the following linear equation for  $U(j, \phi)$ :

$$j \frac{\partial U}{\partial j} - A \frac{\partial U}{\partial \phi} + \frac{\partial^2 U}{\partial \phi^2} + jA \frac{\partial^2 U}{\partial \phi \partial j} + j^2 C \frac{\partial^2 U}{\partial j^2} = 0, \quad (3.12)$$

where

$$A(j, \phi) = \frac{1}{(1+s)} \left[ bs + \frac{p(2+s)\sin 2\phi}{1+p \cos 2\phi} \right], \quad (3.13)$$

$$C(j, \phi) = \frac{1-p(\cos 2\phi - bs \sin 2\phi)}{(1+s)(1+p \cos 2\phi)}. \quad (3.14)$$

Here  $p = (\rho_x - \rho_y) / (\rho_x + \rho_y)$ , and the parameters  $s(j)$  and  $b(\phi)$  are given by Eqs. (2.18). In the isotropic case ( $p = b = 0$ ), Eq. (3.12) reduces to

$$j \frac{\partial U}{\partial j} + \frac{\partial^2 U}{\partial \phi^2} + \frac{j^2}{(1+s)} \frac{\partial^2 U}{\partial j^2} = 0. \quad (3.15)$$

The boundary conditions to Eqs. (3.12) and (3.15) are that the normal components of  $\mathbf{j}$  vanish at the lateral surface of a sample, and the tangential components  $\mathbf{j}_t$  are determined by external conditions, for example, by fixed total current or voltage for a sample connected to an electrical circuit, or by the sweep rate  $\dot{H}_e$  for a superconductor placed in an alternating magnetic field  $H_e(t)$ . In general, these boundary conditions are nonlinear since the requirement that  $\mathbf{j}_t$  is equal to some function  $F(x, y)$  at the surface leads to a nonlinear relation between  $\mathbf{j}_t$  and the coordinates  $x, y$ , which are proportional to the derivatives of  $U$  according to Eqs. (3.9) and (3.10). If the solution of the linear equation (3.12) can be obtained, the stationary distributions of  $H(\mathbf{r})$  and  $\mathbf{j}(\mathbf{r})$  are given by formulas (3.9)–(3.11) which carry out the inverse transformation from the hodograph plane  $(j_x, j_y)$  onto the physical plane  $xy$ . Such a procedure is single valued provided that the Jacobian of the transformation  $\Delta = \partial(x, y) / \partial(\phi, j)$  nowhere passes through zero.<sup>42</sup> As shown in Appendix D, the Jacobian  $\Delta$  is

$$\Delta = jC \left[ \frac{\partial^2 U}{\partial j^2} \right] + \frac{1}{j} \left[ \frac{\partial^2 U}{\partial j \partial \phi} - \frac{1}{j} \frac{\partial U}{\partial \phi} \right] \times \left[ \frac{\partial^2 U}{\partial j \partial \phi} - \frac{1}{j} \frac{\partial U}{\partial \phi} + Aj \frac{\partial^2 U}{\partial j^2} \right], \quad (3.16a)$$

where  $A(\phi, j)$  and  $C(\phi, j)$  are given by Eqs. (3.13) and (3.14). In the isotropic case [ $A=0$ ,  $C=1/(1+s)$ ], Eq. (3.16a) becomes

$$\Delta = \frac{j}{1+s} \left[ \frac{\partial^2 U}{\partial j^2} \right]^2 + \frac{1}{j} \left[ \frac{\partial^2 U}{\partial j \partial \phi} - \frac{1}{j} \frac{\partial U}{\partial \phi} \right]^2. \quad (3.16b)$$

Here the value  $\Delta$  is always positive, and the hodograph transformation is a well-defined procedure since  $s(j) > 0$  for all models discussed in this paper. By contrast, in the anisotropic case the Jacobian  $\Delta$  has no definite sign, which enables one to make definite conclusions about stationary current distributions without solving Eq. (3.12). Indeed, the change of the sign of  $\Delta$  implies that the type of the partial differential equation (3.12) changes from an elliptic ( $\Delta > 0$ ) to a parabolic ( $\Delta < 0$ ) one, which indicates a discontinuity of the current flow under certain conditions.<sup>42</sup> In other words, the condition  $\Delta=0$  is equivalent to the local instability criterion  $s(j(\mathbf{r}))=s_c(\phi(\mathbf{r}))$ , since, at small  $\delta j$ , the hodograph transformation reduces Eq. (3.12) to Eq. (2.13) whose type changes from an elliptic ( $R_2 > 0$ ) to a parabolic ( $R_2 < 0$ ) one when passing through  $s=s_c$ . At  $\Delta > 0$  the stability criterion  $s(j(\mathbf{r})) < s_c(\phi(\mathbf{r}))$  holds everywhere in a sample and the linear equation (3.12) describes a laminar, but generally vortical, current configuration determined by the boundary conditions. Notice that an analysis of even laminar current flow in anisotropic superconductors is a much more complicated problem as compared to the isotropic case since the form of current lines essentially depends on both the sample geometry and the shape and angular dependence of  $\mathbf{E}(\mathbf{j})$  (for example, in an anisotropic cylinder placed in a parallel magnetic field, the current lines are essentially noncircular). In this case the hodograph transformation enables one to simplify the problem considerably since it reduces the nonlinear equation for  $H(x, t)$  to one linear equation for  $U(\mathbf{j})$  at arbitrary  $\mathbf{E}(\mathbf{j})$ .

At  $\Delta < 0$  the situation becomes more complicated since the local instability criterion  $s(j(\mathbf{r})) < s_c(\phi(\mathbf{r}))$  now violates in some regions of the sample. This implies that, under certain conditions, the laminar current flow can break down along the singular lines in the  $xy$  plane, where the tangential components of  $\mathbf{j}$  turn out to be discontinuous. A physical interpretation of this is as follows. We begin first with the isotropic case and notice a formal analogy of Eq. (3.15) with equation which describes a 2D flow of a compressible gas if one replaces  $j \rightarrow v$ ,  $s \rightarrow -v^2/c^2$ ,  $U \rightarrow \Omega$ , where  $\mathbf{v} = -\nabla\Phi$  is a local flow velocity having the potential  $\Phi = \Omega - v\partial_v\Omega$ , and  $c(v)$  is the sound velocity.<sup>42</sup> Let us consider the  $I$ - $V$  curve with a downward curvature ( $s < 0$ ), then the condition that the differential resistivity becomes negative ( $s < -1$ ) corresponds to the transition from subsonic to supersonic regimes in the aerodynamic analogy. On the other hand, the negative differential resistivity is known to result in a stratification of uniform current flow into current domains which are separated by domain walls which match discontinuities of tangential components  $j_t$ .<sup>20-22</sup> A similar situation in aerodynamics occurs when passing through the sound velocity  $v=c$ , which leads to the appearance of shock waves.<sup>42</sup> For instance, the steady-state

equation (3.3) with  $l=0$  reduces to the so-called Euler-Tricomi equation describing low-amplitude shock waves in aerodynamics [some 2D solutions of Eq. (3.3) can be expressed via hypergeometric functions<sup>42</sup>]. Notice that actually the domain walls have a finite width determined by the space dispersion of  $\mathbf{E}(\mathbf{j})$ . As a result, the tangential component of  $\mathbf{j}$  sharply varies within the domain wall over the length  $l$ , the macroscopic approach based on the hodograph transformation corresponding to the limit  $l \rightarrow 0$ .

In the anisotropic case, one can therefore interpret Eq. (3.12) in terms of a compressible flow of magnetic flux having an anisotropic nonlinear viscosity. Then the instability at  $s=s_c$  corresponds to the vanishing of this viscosity along the  $\zeta$  axis, which results in a generation of the current domain walls. Their appearance is due to the hysteretic form of the  $I$ - $V$  curve shown in Fig. 11, where the domain wall corresponds to a jump in  $j_\zeta$  caused by a switching between the raising branches of the  $N$ -shaped function  $E_\zeta(j_\zeta)$  (see, e.g., Refs. 20-22). Due to the essential effect of the boundary conditions, these domain walls are curved and form the network sketched in Fig. 13. A mathematical description of such a structure can be very complicated, for example, an analysis of similar problems in a theory of dendritic crystal growth,<sup>44</sup> as well as the hydrodynamics of a 2D viscous two-phase flow<sup>43</sup> or liquid crystals,<sup>15</sup> indicates instabilities of flat interfaces resulting in nontrivial chaotic patterns.

Therefore, the finite-amplitude structures at  $s > s_c$  could be treated as a cellular current pattern formed by a network of curved domain walls of thickness  $\sim l$ . Notice that the formation of such a network, which depends on the sample geometry, makes the initially potential current rotational flow, by analogy with hydrodynamics, where a potential stream becomes a rotational flow upon passing through curved shock waves.<sup>42</sup> This results in a partial closure of current lines and appearance of anisotropic current loops within the current grains in Fig. 13. Such grains can be treated as magnetic macroscopic vortices in the system of Abrikosov vortices.<sup>10</sup> Qualitatively, the formation of the macroscopic vortex structure was discussed above when considering the current fragmentation in a slab in Fig. 9.

Sizes of the macroscopic vortices and densities of closed currents  $j_s$ , circulating within them, essentially depend on  $j$  and the relation between  $s(j)$  and  $s_c(\phi)$ . For the macroscopic vortices much larger than  $l$ , the condition of the local stability reads  $s(j(\mathbf{r})) < s_c(\phi(\mathbf{r}))$  every-

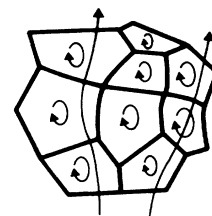


FIG. 13. A fragment of current granular state. The full and thin curves show domain walls and current lines, respectively.

where within the macroscopic vortex. If such a structure appears upon increasing  $J$  above  $j_{f1}$ , then the condition  $s < s_c$  can be fulfilled provided that  $j_s > j_{f2}(\phi) \sim j_c$ . This is a lower estimation of  $j_s$  which ensures the local stability of circulating currents when they flow along the direction  $\phi = \phi_m$  corresponding to the minimum of  $s_c(\phi)$  in Fig. 4. Thus, an increase of  $j$  above  $j_{f1}$  leads to a jump-wise appearance of local vortical currents  $j_s \sim j_{f2} - j_{f1}$ . The amplitude  $j_s$  decreases upon approaching the critical point  $s = s_c(\phi_t)$ ,  $\phi = \phi_t$ , where the kinetic transition becomes nearly of second order. Here  $j_s \ll j$  and the character of the current patterns changes from the macroscopic vortex structure to weak modulations of  $\mathbf{j}(\mathbf{r})$ .

Spatial scales of current modulation are maximum near the critical point, where they seem to be of the order of the transversal sizes of a sample. The growth of the control parameter  $\epsilon$  leads to a successive fragmentation of large macroscopic vortices into smaller ones because of the appearance of new domain walls, which is accompanied by an increase of amplitudes of screening currents circulating within the macroscopic vortices. This process begins with large macroscopic vortices and finally results in macroscopic vortices comparable with the microscopic length  $l$  at  $s \gg s_c$ . In this scenario the current patterns are assumed to be stationary and the vorticity of  $\mathbf{j}$  comes from the crystalline anisotropy and the curvature of the domain walls. However, one cannot exclude a possibility of dynamic large-amplitude structures as well, for example, local oscillations of the macroscopic vortices and their viscous motion caused by the Lorentz force. Notice that both situations have some "hydrodynamic" analogs in the physics of liquid crystals, where the spontaneous generation of domain walls due to the field-induced orientational instability can result in both stationary and dynamic structures.<sup>15</sup>

#### IV. DISCUSSION

##### A. Resistive transition

Now we discuss possible manifestations of the electromagnetic instability, in particular, the resistive transition occurring at  $j = j_{f1}$ . As shown above, the instability can result in the essential growth of total electric resistance because of the increase of the amplitudes of local vortical currents at  $j > j_{f1}$ . Characteristic current densities within the macrovortices are of order  $j_c$ , with a dissipation corresponding rather to the viscous flux flow. This manifests itself as a resistive transition similar to that from the flux-creep to flux-flow regimes, with the value  $j_{f1}$  playing the role of a "critical" current density. However, that  $j_{f1}$  has a dynamic origin and can be well below  $j_c$  determined by a static balance of pinning and Lorentz forces (see, e.g., Ref. 45). Let us consider as an illustration the case of currents flowing in the ac plane of high- $T_c$  superconductors where the anisotropy is the most pronounced. Assuming  $\rho_x \gg \rho_y$ ,  $x = c$ ,  $y = a$  in Eq. (2.34), and taking  $\rho_s \sim 0.1\rho_c$  for  $\text{YBa}_2\text{Cu}_3\text{O}_7$ , or  $\rho_a \sim (10^{-4} - 10^{-5})\rho_s$  for Bi- or Tl-based compounds, and  $j_1 \sim (10^{-1} - 10^{-2})j_c$ ,<sup>27-31</sup> one finds that  $j_{f1} \sim (10^{-1} - 10^{-2})j_c$ .

Thus, the anisotropy can considerably reduce the current-carrying capacity which is now determined not by the pinning force itself but rather by details of  $\mathbf{E}(\mathbf{j})$  deep within the flux-creep region. Notice the specific angular dependence of  $j_{f1}(\phi)$  which reveals sharp peaks at  $\phi = \pi n / 2$  (Fig. 5). The amplitudes of the peaks are limited by the corresponding values of  $j_c(\phi)$ , since the uniform resistive state is stable if the angles of  $\mathbf{j}$  with the  $x$  or  $y$  axes are smaller than  $\phi_c \sim (\rho_y j_1 / \rho_x j_c)^{1/2} \ll 1$ . At the same time, there is a wide region of  $\phi$  for which  $j_{f1} \ll j_c$ , regardless of specific mechanisms of pinning. Similar angular dependences of critical current and conductivity have been observed in thin films and bulk high- $T_c$  superconductors upon varying the field direction with respect to the  $c$  axis<sup>28-30</sup> and in grain-oriented  $\text{YBa}_2\text{Cu}_3\text{O}_7$  when changing the angle between the transport current and the  $ab$  plane.<sup>31</sup> Herewith, the angular dependence of  $j_{f1}(\phi) \propto |\cos\phi|^{-1/2}$  at  $\phi \approx \pi n / 2$  is similar to that of the intrinsic pinning model.<sup>46</sup>

The fragmentation of the uniform resistive state should be the most pronounced for perfect anisotropic single crystals, especially for Bi- and Tl based compounds. A nonlinear resistivity of the macroscopic vortex state seems to be calculated only within the framework of microscopic models of flux dynamics. In any case, however, the appearance of the macroscopic vortex structure decreases the nonlinearity and anisotropy of the average  $\mathbf{E}(\mathbf{j})$  compared with the local  $\mathbf{E}(\mathbf{j})$ . Indeed, in the long-wavelength limit  $k \rightarrow 0$ , the steady-state current structure could be treated as some effective medium with renormalized parameters  $\hat{s}(j)$  and  $\hat{s}_c(\phi)$ . Then the stability criterion of the macroscopic vortex state  $\hat{s} < \hat{s}_c$  implies that such a medium is more macroscopically isotropic and "linear" than the initially unstable uniform state. These arguments allow one to suggest that the  $I$ - $V$  curves of highly anisotropic superconductors are linear, except for currents nearly parallel to the symmetry axes. Likewise, the macroscopic anisotropy could be reduced by any random inhomogeneities, which also results in the suppression of the long-wavelength instability.

The electromagnetic instability can be treated as a current-induced kinetic transition from the laminar flux-creep to vortical flux-creep or flux-flow regimes. This manifests itself in singularities of a dynamical response of the current state, for example, in an increase of the electric noise power upon approaching  $j_{f1}$ . Let us consider an equilibrium part of the noise by separating current fluctuations into statistically independent components  $\delta j_\xi$  and  $\delta j_\eta$ . Making use of the Nyquist theorem, one gets the power spectra  $\langle \delta j_\xi^2 \rangle_\omega$  and  $\langle \delta j_\eta^2 \rangle_\omega$  in the form

$$\langle \delta j_\xi^2 \rangle_\omega = 2k_B T / VR_2(j), \quad \langle \delta j_\eta^2 \rangle_\omega = 2k_B T / VR_1(j), \quad (4.1)$$

where  $V$  is the volume of a sample, and  $R_{1,2}$  are given by Eq. (2.14). Here  $R_1$  remains finite at  $j = j_{f1}$ , whereas  $R_2 \propto (j_{f1} - j)$  passes through zero. At the instability threshold, the current fluctuations become highly anisotropic due to the divergence of  $\langle \delta j_\xi^2 \rangle_\omega \propto 1 / (j_{f1} - j)$ , where  $j_{f1}(\phi)$  essentially depends on the orientation of the

transport current. This also may lead to a peak of mechanical damping in vibrating-reed experiments which could be due to neither the flux line melting<sup>47,48</sup> nor the depinning transition.<sup>49,50</sup>

### B. Magnetization and self-induced magnetic granularity

Manifestations of the instability in irreversible magnetic properties of anisotropic superconductors are due to the above-discussed breakdown of the laminar Bean-like configuration of magnetization currents which turns into a granular current state with large intragrain screening currents at comparatively low value of macroscopic  $j$  (see Fig. 13). The boundaries of the current grains (macroscopic vortices) are the domain walls of thickness  $l$ , within which a sharp variation of tangential component of  $\mathbf{j}$  occurs. Magnetic properties of such a state prove to be similar to those of ceramic superconductors in which crystalline grains are coupled by weak Josephson interaction (see, e.g., Refs. 36–39). In both cases there are two current systems corresponding to high local currents ( $j \sim j_s$ ) circulating within the grains and low macroscopic currents flowing through the grain boundaries ( $j \sim j_{f1}$ ). This leads to a magnetic granularity which was observed on both ceramic and grain-oriented and single-crystalline high- $T_c$  superconductors.<sup>38,39</sup> The magnetic granularity is usually attributed to the crystalline granularity caused by various structural defects (grain boundaries, stacking faults, twins, etc.) which are assumed to exhibit weak-link properties because of the short coherence length.<sup>51</sup> These inherent weak links essentially reduce the intergrain  $j_c$  compared with the intragrain one.

The appearance of the macroscopic vortex structure may be another mechanism of the magnetic granularity arising without weak links. As follows from the above analysis, this mechanism should be the most pronounced in anisotropic single crystals, especially in Bi- or Tl-based superconductors. Here the current domain walls play the role of self-induced weak links whose form and distribution depend on induced electric fields, sample geometry, form of  $\mathbf{E}(\mathbf{j})$  in the flux-creep regime, etc. This leads to a self-induced magnetic granularity determined not by the weak-link structure, but rather the nonlinearity of  $\mathbf{E}(\mathbf{j})$  at  $j < j_c$ .<sup>53</sup> Since the shape of  $\mathbf{E}(\mathbf{j})$  essentially depends on  $T$  and  $B$ , the magnetic granularity turns out to be very sensitive to changes of  $T$  and  $B$  as well. For instance, above the irreversibility line,<sup>14</sup> the nonlinearity of  $\mathbf{E}(\mathbf{j})$  decreases considerably, thereby the macroscopic vortex structure could exist only at high anisotropy.

Another possibility to reveal the self-induced magnetic granularity could be measurements of  $M$  of anisotropic superconductors placed in an alternating magnetic field  $H_e(t)$ , or a decay of the remanent  $M(t)$  at fixed  $H_e$  (flux creep). In the first case, the electric field in a sample is proportional to  $\dot{B}_e$ , for example,  $E_\phi = \dot{B}_e r/2$  for a long cylinder parallel to  $\mathbf{H}$ . Such a field induces the electric currents

$$j(\mathbf{r}) \simeq \{1 - (k_B T/U) \ln[E_c/E(\mathbf{r})]\} j_c$$

close by  $j_c$  with an accuracy to a small ratio  $k_B T/U$  over

a wide region of the parameters ( $E_c$  is a crossover electric field between the flux-flow and flux-creep regimes). However, for highly anisotropic superconductors the difference  $j_c - j_{f1}$  can be of order  $j_c$ , thereby the local instability of laminar current configurations can occur in the regions where  $s(j(\mathbf{r})) > s_c(\phi(\mathbf{r}))$  practically at any  $T$  and  $B$ . This implies that the total magnetic moment essentially depends on the distribution of the macroscopic vortices determined by the sweep rate and the sample geometry.

In the flux-creep experiments, the field  $H_e(t)$  is increased up to a certain value  $H_e(0)$  and then kept fixed, which leads to a decay of induced magnetization currents at  $t > 0$  due to a nonzero resistivity at  $j < j_c$ . If the initial value of  $j(t)$  is close by  $j_c$ , then the self-induced granularity arises during a time interval  $0 < t < t_c(T, B)$ , where  $t_c(T, B)$  is the time needed for a decay of  $j(t)$  from  $j \simeq j_c$  to the minimum value  $j_m = j_{f1}(\phi_m)$  at which the existence of the macroscopic vortices is still possible. The fraction of the sample occupied by the macroscopic vortices decreases with  $t$  such that, at  $t > t_c(T, B)$  the current flow becomes laminar. However, due to the specific angular dependence of  $j_{f1}(\phi)$  (Fig. 5), the current distribution even at  $t > t_c$  essentially differs from that shown in Fig. 9(a).

As an illustration, we consider a slab placed in the magnetic field  $\mathbf{H}$  perpendicular to the anisotropic  $xy$  plane, restricting ourselves to the strong anisotropy limit  $j_m \ll j_c(\phi)$ . Shown in Fig. 14 is a possible laminar current configuration at  $t > t_c$ , which differs from that in Fig. 9(a) in that the singular lines turn into four overlapping sectors, where the current density equals  $j_m$  and makes the angles  $\pm\phi_m$  with the  $x$  axis. In contrast to the case presented in Fig. 9(a), the lines where the current sharply changes direction do not already play the role of the self-induced weak links since  $\mathbf{j}$  flowing through them exceeds  $j_m$ . As a result, the above-discussed splitting of current loops does not occur, which indicates the distribution is stable. A direct calculation of the magnetic moment  $M$  for the case shown in Fig. 14 yields

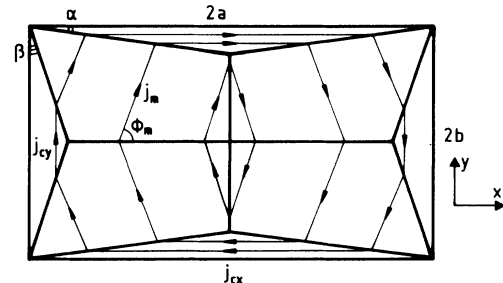


FIG. 14. An example of stable Bean-like current configuration in an anisotropic slab. The thick and thin lines show singular and current lines, respectively. The angles  $\alpha$  and  $\beta$  are determined by the continuity of normal components of  $\mathbf{j}$  through the singular lines as follows  $\tan\alpha = j_m \sin\phi_m / (j_{cx} - j_m \cos\phi_m)$  and  $\tan\beta = j_m \cos\phi_m / (j_{cy} - j_m \sin\phi_m)$ , where  $j_{cx}$  and  $j_{cy}$  are the critical current densities along the  $x$  and  $y$  axes, respectively.

$$M = 0.5 \int [\mathbf{r} \times \mathbf{j}]_z dx dy$$

$$= 2abj_m (b \cos \phi_m + a \sin \phi_m). \quad (4.2)$$

This formula is valid in the strong anisotropy limit  $j_m \ll j_c(\phi)$  for which the triangular regions where the currents flow parallel to the  $x$  and  $y$  axes give the same contribution to  $M$  as the butterflylike domain, where  $j = j_m$ . The field of the full flux penetration into the sample is

$$H_p = j_m (b \cos \phi_m + a \sin \phi_m). \quad (4.3)$$

Here neither  $M$  nor  $H_p$  depend on  $j_c$  along the symmetry axes. In particular, the measurements of  $M$  for  $H \parallel ab$  in highly anisotropic Bi- or Bi-based high- $T_c$  superconductors may give only the combination  $(b \cos \phi_m + a \sin \phi_m)j_m$ , but do not enable one to extract  $j_{cx}$  and  $j_{cy}$ .

An estimation of the time  $t_c(T, B)$  is very sensitive to details of  $\mathbf{E}(\mathbf{j})$  in the flux-creep regime. Let us consider here the simplest case of the exponential  $I$ - $V$  curve  $E \propto \exp[(j - j_c)/j_1]$  which results in the logarithmic decay  $j(t) = j_c - j_1 \ln(t/t_0)$ , where  $j_1(T, B) = -dj/d \ln t$  is an observed flux-creep rate,  $t_0 \sim \mu_0 L^2 / \rho_f$  is a time constant,<sup>54-56</sup> and  $L$  is a sample size. Hence,

$$t_c \sim t_0 \exp[(j_c - j_{f1})/j_1]. \quad (4.4)$$

Taking  $L \sim 0.1$  mm,  $\rho_f \sim 10 \mu \Omega \text{cm}$ ,  $j_c/j_1 \simeq 40$ ,<sup>39</sup> one finds  $t_0 \sim 10^{-7}$  s, and  $t_c \sim 3$  ms at  $j_{f1} = 0.8j_c$  and  $t_c \sim 3 \times 10^4$  s at  $j_{f1} = 0.4j_c$ . Therefore, at a moderate anisotropy ( $j_{f1} \simeq j_c$ ), the macroscopic vortices arising at initial stages of the flux creep disappear for a short time much smaller than typical experimental time windows

$$u = (n_y^2 + n_z^2)R_{xx} + (n_x^2 + n_z^2)R_{yy} + (n_y^2 + n_x^2)R_{zz}$$

$$- (R_{xy} + R_{yx})n_x n_y - (R_{xz} + R_{zx})n_x n_z - (R_{yz} + R_{zy})n_y n_z, \quad (A2)$$

$$v = (R_{yy}R_{zz} - R_{yz}R_{zy})n_x^2 + (R_{xx}R_{zz} - R_{xz}R_{zx})n_y^2 + (R_{xx}R_{yy} - R_{xy}R_{yx})n_z^2$$

$$+ [R_{zx}R_{yz} + R_{xz}R_{zy} - (R_{xy} + R_{yx})R_{zz}]n_x n_y$$

$$+ [R_{xy}R_{yz} + R_{yx}R_{zy} - (R_{xz} + R_{zx})R_{yy}]n_x n_z + [R_{xz}R_{yx} + R_{zx}R_{xy} - (R_{yz} + R_{zy})R_{xx}]n_x n_z. \quad (A3)$$

Formulas (A1)–(A3) describe two modes, unlike the 2D case in which there is only one mode given by Eq. (2.9). Another feature of the 3D case is a possibility of oscillation at  $u^2 < 4v$ . The spectrum  $\lambda(\mathbf{k})$  simplifies if currents flow along a symmetry plane, say,  $\mathbf{j} \parallel xy$  and  $\mathbf{B} \parallel z$ . Then the elements  $R_{xz}$ ,  $R_{zx}$ ,  $R_{yz}$ , and  $R_{zy}$  vanish due to symmetry and Eq. (A1) reduces to that of Ref. 10.

#### APPENDIX B: CALCULATION OF $N$ AND $\epsilon$

In order to get  $N$ , we expand  $\mathbf{E}$  up to second-order terms in  $\delta \mathbf{j}$  as follows:

$\Delta t \sim 10^3 - 10^5$  s and do not affect the observed relaxation of  $M(t)$ . However, highly anisotropic superconductors ( $j_{f1} \ll j_c$ ,  $t_c > \Delta t$ ) can reveal the magnetic granularity caused by the frozen macroscopic vortex structure within the entire time window  $\Delta t$ .

If the field  $\mathbf{H}_e$  is inclined with respect to the symmetry axes, the formation of the macroscopic vortex structure can change both the value and the direction of  $\mathbf{M}$ , which results in a torque. This may manifest itself in peculiarities of the torque flux creep<sup>57</sup> or hysteretic jumpwise changes of the direction of  $\mathbf{M}$  in a superconductor placed in a rotating magnetic field.<sup>58</sup> Such a behavior is a result of the  $N$ -shaped  $I$ - $V$  curve shown in Fig. 11.

#### ACKNOWLEDGMENTS

I am grateful to E. H. Brandt, J. R. Clem, J. E. Evetts, P. H. Kes, V. G. Kogan, H. Küpfer, and D. C. Larbalestier for useful discussions. I thank the Institute of Technical Physics for hospitality during my stay. This work was partly supported by the Alexander von Humboldt Foundation, and also DARPA, and Electric Power Institute.

#### APPENDIX A: 3D SPECTRUM

The cubic secular equation (2.6) actually reduces to a quadratic one since Eq. (2.6) automatically gives  $\text{div} \delta \mathbf{j} = 0$  or  $\mathbf{k} \delta \mathbf{j}(\mathbf{k}) = 0$ . A direct evaluation of the determinant (2.6) yields

$$f_{\pm} = u/2 \pm (u^2/4 - v)^{1/2}, \quad (A1)$$

where the functions  $u(\mathbf{n})$  and  $v(\mathbf{n})$  are given by

$$\delta E_{\alpha} = R_{\alpha\beta} \delta j_{\beta} + \frac{1}{2} \delta j_{\beta} \delta j_{\gamma} \frac{\partial R_{\alpha\beta}}{\partial j_{\gamma}}. \quad (B1)$$

In the coordinate frame  $(\zeta, \eta)$ , Eq. (B1) reads

$$\delta E_{\zeta} = R_2 \delta j_{\zeta} + \frac{1}{2} \left[ \frac{\partial R_2}{\partial j_{\zeta}} \delta j_{\zeta} + \frac{\partial R_2}{\partial j_{\eta}} \delta j_{\eta} \right] \delta j_{\zeta} \quad (B2)$$

(with no summation over  $\zeta$  and  $\eta$ ). Hence, it follows that  $N = \frac{1}{2} \partial R_2 / \partial j_{\zeta}$ , with

$$R_2 = [4R_{xx}R_{yy} - (R_{xy} + R_{yx})^2] / 2R_1.$$

Making use of Eqs. (2.15), the formula for  $R_2(s)$  at  $s \simeq s_c$

can be written as

$$R_2 = R_0(\phi)[s_c(\phi) - s] , \tag{B3}$$

$$R_0(\phi) = \frac{4\rho_x\rho_y(g^2 + 4g)^{1/2}G}{(\rho_x + \rho_y)(2 + s_c) + s_c(\rho_x - \rho_y)(\cos 2\phi + b \sin 2\phi)} . \tag{B4}$$

Furthermore, one has

$$2N = \frac{\partial R_2}{\partial j} \frac{\partial j}{\partial j_\xi} + \frac{\partial R_2}{\partial \phi} \frac{\partial \phi}{\partial j_\xi} . \tag{B5}$$

Here  $j_\eta = j \sin(\phi + \psi)$  and  $j_\xi = -j \cos(\phi + \psi)$  (see Fig. 2), hence,

$$\frac{\partial j}{\partial j_\xi} = -\cos(\phi + \psi), \quad \frac{\partial \phi}{\partial j_\xi} = \frac{1}{j} \sin(\phi + \psi) - \frac{\partial \psi}{\partial j_\xi} \tag{B6}$$

with  $\psi$  given by Eqs. (2.11) and (2.19), and

$$\partial \psi / \partial j_\xi = (\partial \psi / \partial j)(\partial j / \partial j_\xi) + (\partial \psi / \partial \phi)(\partial \phi / \partial j_\xi) .$$

Inserting the derivatives into Eq. (B5) and differentiating  $R_2$ , at  $s \rightarrow s_c$  one finally obtains

$$N = \left[ \cos \chi \frac{\partial s}{\partial j} + \frac{\partial s_c}{\partial \phi} \left[ \frac{1}{j} \sin \chi + \frac{(\partial \psi / \partial j) \cos \chi}{1 + (\partial \psi / \partial \phi)} \right] \right] R_0 , \tag{B7}$$

where  $\chi = \phi + \psi$  is determined by Eqs. (2.16)–(2.19). Assuming  $N = 0$ , one gets Eq. (3.8).

The formula for  $\epsilon = -R_2/R_1$  can be obtained from Eqs. (B3) and (B5) as follows:

$$\epsilon = (s - s_c)\epsilon_0 , \tag{B8}$$

$$\epsilon_0 = \frac{4\rho_x\rho_y(g^2 + 4g)^{1/2}G}{[(\rho_x + \rho_y)(2 + s_c) + s_c(\rho_x - \rho_y)(\cos 2\phi + b \sin 2\phi)]^2} . \tag{B9}$$

**APPENDIX C: STATIONARY 1D SOLUTIONS OF EQ. (3.3)**

At  $\partial_t h = \partial_\xi h = 0$ , Eq. (3.3) after double integration over  $\eta$  reduces to

$$l^2 u'' + \epsilon u - u^2 = 0 , \tag{C1}$$

where  $u = h'$ , and the prime denotes the differentiation with respect to  $\eta$ . Here we put the integration constants zero in order to ensure the correct uniform state  $u = 0$ . Multiplication of Eq. (C1) by  $u'$  and integration over  $\eta$  give

$$l^2 u'^2 = 2u^3/3 - \epsilon u^2 + C , \tag{C2}$$

where  $C$  will be determined below. Solutions of Eq. (C2) can be written as an integral

$$\eta = l(\frac{3}{2})^{1/2} \int_{u_1}^u [(x - u_1)(x - u_2)(x - u_3)]^{-1/2} dx , \tag{C3}$$

which can be expressed via elliptic functions. Here

$u_1 < u_2 < u_3$  are the roots of the cubic equation (C2) with  $u' = 0$ ; moreover,

$$u_1 + u_2 + u_3 = 3\frac{\epsilon}{2} , \tag{C4}$$

$$u_1 u_2 + u_1 u_3 + u_2 u_3 = 0 . \tag{C5}$$

The critical nucleus corresponds to the solution of  $u(\eta)$  of Eq. (C2) for which  $u(\pm\infty) = u'(\pm\infty) = 0$  and  $C = 0$ . Such a solution described by Eq. (3.6) exists only if  $\epsilon < 0$ .

Now we turn to periodic solutions of Eq. (C1) obeying Eq. (3.1) which read

$$\int_{u_1}^{u_2} [(x - u_1)(x - u_2)(x - u_3)]^{-1/2} x dx = 0 . \tag{C6}$$

This condition can be expressed in terms of complete elliptic integrals  $K(m)$  and  $E(m)$  (Ref. 52) as

$$u_1 E(m) + [K(m) - E(m)]u_3 = 0 , \tag{C7}$$

$$(1 - m)u_1 - u_2 + mu_3 = 0 . \tag{C8}$$

Solving linear equations (C4), (C7), and (C8) and substituting the result into Eq. (C5), one finds the following equation for the parameter  $0 < m < 1$ :

$$3E^2(m) - 2E(m)K(m)(2 - m) + (1 - m)K^2(m) = 0 . \tag{C9}$$

This equation has the only solution  $m = 0$  which does not correspond to the periodic function obeying Eq. (3.1).

**APPENDIX D: HODOGRAPH TRANSFORMATION**

In the 2D case, the stationary Maxwell equations

$$\partial_x E_y - \partial_y E_x = 0 , \tag{D1}$$

$$j_x = \partial_y H, \quad j_y = -\partial_x H \tag{D2}$$

with  $\mathbf{E} = \mathbf{E}(\mathbf{j})$  reduce to one nonlinear equation for  $H(x, y)$ . Making use of the Legendre transformation, it is convenient to transform from the independent variables  $x$  and  $y$  to new variables  $j_x$  and  $j_y$  by presenting Eq. (D2) as

$$dH = d(jy_x) - d(xj_y) - ydj_x + xdj_y . \tag{D3}$$

Let us introduce the function

$$U = H + xj_y - yj_x \tag{D4}$$

such that  $dU = xdj_y - ydj_x$  and

$$x = \frac{\partial U}{\partial j_y}, \quad y = -\frac{\partial U}{\partial j_x} , \tag{D5}$$

where  $U(\mathbf{j})$  is regarded as a function of  $\mathbf{j}$ . Assuming  $j_x = j \cos \phi$  and  $j_y = j \sin \phi$ , we get formulas (3.9) and (3.10) instead of Eqs. (D5). To express Eqs. (D1) and (D2) through the variables  $j$  and  $\phi$ , it is convenient to write Eq. (D1) as Jacobians:<sup>42</sup>

$$\frac{\partial(E_x, x)}{\partial(x, y)} + \frac{\partial(E_y, y)}{\partial(x, y)} = 0 . \tag{D6}$$

Multiplying Eq. (D6) by the Jacobian  $\Delta = \partial(x, y) / \partial(j, \phi)$ , one finds

$$\frac{\partial E_y}{\partial j} \frac{\partial y}{\partial \phi} - \frac{\partial E_y}{\partial \phi} \frac{\partial y}{\partial j} + \frac{\partial E_x}{\partial j} \frac{\partial x}{\partial \phi} - \frac{\partial E_x}{\partial \phi} \frac{\partial x}{\partial j} = 0. \quad (\text{D7})$$

Taking  $E_x = \rho_x j G(j/j_k(\phi)) \cos \phi$ ,  $E_y = \rho_y j G(j/j_k(\phi)) \sin \phi$ , and making use of Eqs. (3.15), one gets after some algebra the linear equation (3.12) for  $U(j, \phi)$ .

The hodograph transformation is a well-defined procedure provided that the Jacobian  $\Delta$  is nowhere zero. A direct calculation of  $\Delta$  by means of Eqs. (3.9) and (3.10) gives

$$\Delta = \frac{1}{j} \left[ \frac{\partial^2 U}{\partial j \partial \phi} - \frac{1}{j} \frac{\partial U}{\partial \phi} \right]^2 - \left[ \frac{\partial U}{\partial j} + \frac{1}{j} \frac{\partial U}{\partial \phi} \right] \frac{\partial^2 U}{\partial j^2}. \quad (\text{D8})$$

By expressing the combination  $\partial_j U + j^{-1} \partial_\phi U$  by Eq. (3.12), one finds Eqs. (3.16a) and (3.16b). A similar hodograph transformation can be used if the stationary Maxwell equations are written in terms of the scalar potential  $\Phi$  such that  $\mathbf{E} = -\nabla \Phi$ . Then one can introduce a function  $U(\mathbf{E})$  for which  $\mathbf{r} = \nabla_{\mathbf{E}} U$ , and  $\Phi = U - E \partial U / \partial E$ . In this case the condition  $\text{div}(\mathbf{j}(\mathbf{E})) = 0$  gives a linear equation for  $U(\mathbf{E})$  in the same way as discussed above. Such a representation could be convenient for the analysis of 3D current configurations.

\*Present address.

- <sup>1</sup>V. G. Kogan, Phys. Rev. Lett. **64**, 2192 (1990); A. M. Grishin, A. Yu. Martynovich, and S. V. Yampol'skii, Zh. Eksp. Teor. Fiz. **97**, 1930 (1990) [Sov. Phys. JETP **70**, 1089 (1990)]; A. I. Buzdin and A. Yu. Simonov, Physica C **168**, 421 (1990).
- <sup>2</sup>P. H. Kes, J. Aarts, V. M. Vinokur, and C. J. van der Beek, Phys. Rev. Lett. **64**, 1063 (1990).
- <sup>3</sup>J. R. Clem, Phys. Rev. B **43**, 7837 (1991).
- <sup>4</sup>E. H. Brandt, Phys. Rev. Lett. **63**, 1106 (1989); A. Houghton, R. A. Pelcovits, and A. Sudbø, Phys. Rev. B **40**, 6763 (1989).
- <sup>5</sup>As reviews, see, e.g., S. Doniach, in *High Temperature Superconductivity*, Proceedings of the Los Alamos Symposium, 1989, edited by K. S. Bedell *et al.* (Addison-Wesley, Redmond City, 1990), p. 406; E. H. Brandt, Int. J. Mod. Phys. **5**, 751 (1991).
- <sup>6</sup>D. R. Nelson and H. S. Seung, Phys. Rev. B **39**, 9174 (1989); M. S. Marchetti and D. R. Nelson, *ibid.* **41**, 1910 (1990).
- <sup>7</sup>M. Tinkham, Phys. Rev. Lett. **61**, 1658 (1988); Helv. Phys. Acta **61**, 443 (1988).
- <sup>8</sup>M. P. A. Fisher, Phys. Rev. Lett. **62**, 1415 (1989); D. S. Fisher, M. P. A. Fisher, and D. A. Huse, Phys. Rev. B **43**, 130 (1991).
- <sup>9</sup>G. Blatter, V. B. Geshkenbein, and A. I. Larkin, Phys. Rev. Lett. **68**, 875 (1992).
- <sup>10</sup>A. Gurevich, Phys. Rev. Lett. **65**, 3197 (1990).
- <sup>11</sup>E. M. Gyorgy, R. B. van Dover, K. A. Jackson, L. F. Schneemeyer, and J. V. Waszczak, Appl. Phys. Lett. **55**, 283 (1989); R. L. Peterson, J. Appl. Phys. **67**, 6930 (1990).
- <sup>12</sup>M. V. Feigel'man, V. G. Geshkenbein, A. I. Larkin, and V. M. Vinokur, Phys. Rev. Lett. **63**, 2309 (1989); K. H. Fisher and T. Nattermann, Phys. Rev. B **43**, 10372 (1991).
- <sup>13</sup>M. Tinkham, *Introduction to Superconductivity* (McGraw-Hill, New York, 1975).
- <sup>14</sup>K. A. Muller, M. Takashige, and J. G. Bednorz, Phys. Rev. Lett. **58**, 1143 (1987); Y. Yeshurun and A. P. Malozemoff, *ibid.* **60**, 2202 (1988).
- <sup>15</sup>P. G. de Gennes, *The Physics of Liquid Crystals* (Clarendon, Oxford, 1975).
- <sup>16</sup>E. Zeldov, N. M. Amer, G. Koren, A. Gupta, R. J. Gambino, and M. W. McElfresh, Phys. Rev. Lett. **62**, 3093 (1989); E. Zeldov, N. M. Amer, G. Koren, and A. Gupta, Appl. Phys. Lett. **56**, 1700 (1990); H. J. Jensen and P. Minnhagen, Phys. Rev. Lett. **66**, 1630 (1991).
- <sup>17</sup>J. E. Ekin, H. R. Hart, and A. R. Gaddipati, J. Appl. Phys. **68**, 2285 (1990); J. Z. Sun, C. B. Eom, B. Larison, J. C. Bravman, and T. Geballe, Phys. Rev. B **43**, 3002 (1991).
- <sup>18</sup>A. I. Larkin and Yu. N. Ovchinnikov, in *Modern Problems in*

*Condensed Matter Sciences*, edited by D. N. Lancenberg and A. I. Larkin (North-Holland, Amsterdam, 1986), Vol. 12, p. 493.

- <sup>19</sup>The self-field effects are due to the explicit dependence of  $\mathbf{E}(\mathbf{j})$  upon  $B$ . As a result, the tensor  $R_{\alpha\beta}$  becomes dependent on  $\mathbf{r}$ , since  $\delta E_\alpha = R_{\alpha\beta}(B, \mathbf{j}) \delta j_\beta + (\partial E_\alpha / \partial B) \delta B$ , where  $B(\mathbf{x}) = B_e + \mu_0 \mathbf{j} \cdot \mathbf{x}$ . However, such a dependence, as well as the term  $(\partial E_\alpha / \partial B) \delta B$  resulting in additional "magnetic" anisotropy can be neglected in the case of strong external fields  $B_e \gg jL$  and high crystalline anisotropy considered in this paper since the most unstable electromagnetic modes correspond to wavelengths much shorter than a transversal sample size  $L$ .
- <sup>20</sup>K. Seeger, *Semiconductor Physics* (Springer-Verlag, Berlin, 1982).
- <sup>21</sup>H. Haken, *Synergetics. An Introduction* (Springer-Verlag, Berlin, 1978).
- <sup>22</sup>A. V. Gurevich and R. G. Mints, Rev. Mod. Phys. **59**, 941 (1987).
- <sup>23</sup>A similar instability also arises in more obvious case of  $G(j)$  decreasing with  $j$ , i.e.,  $s(j) < 0$ . Here the instability criterion reads  $s < s_c$ , where  $s_c$  is given by Eq. (2.16) with the negative sign in front of the square root.
- <sup>24</sup>D. Dew-Hughes, Cryogenics **28**, 647 (1988); P. H. Kes, J. Aarts, J. van der Berg, C. J. van der Beek, and J. A. Mydosh, Supercond. Sci. Technol. **1**, 242 (1989).
- <sup>25</sup>Y. Iye, S. Nakamura, and T. Tamegai, Physica C **159**, 616 (1989).
- <sup>26</sup>M. V. Feigel'man, V. B. Geshkenbein, and A. I. Larkin, Physica C **167**, 177 (1990); V. M. Vinokur, P. H. Kes, and A. E. Koshelev, *ibid.* **168**, 28 (1990).
- <sup>27</sup>S. Martin, A. T. Fiory, R. M. Fleming, G. P. Espinosa, and A. S. Cooper, Appl. Phys. Lett. **54**, 72 (1989).
- <sup>28</sup>B. Roas, L. Shultz, and G. Saemann-Ischenko, Phys. Rev. Lett. **64**, 479 (1990).
- <sup>29</sup>T. T. M. Palstra, B. Batlogg, R. B. van Dover, L. F. Schneemeyer, and J. V. Waszczak, Phys. Rev. B **41**, 6621 (1990).
- <sup>30</sup>Y. Iye, S. Nakamura, T. Tamegai, T. Terashima, K. Yamamoto, and Y. Bando, Physica C **166**, 62 (1990).
- <sup>31</sup>V. Selvamanickam and K. Salama, Appl. Phys. Lett. **57**, 1575 (1990).
- <sup>32</sup>J. W. Cahn, J. Chem. Phys. **42**, 93 (1965); A. G. Khachatryan, *Theory of Structural Transformations in Solids* (Wiley, New York, 1983).
- <sup>33</sup>J. Clarke, in *Nonequilibrium Superconductivity, Phonons and*

- Kapitza Boundaries*, edited by K. E. Gray (Plenum, New York, 1981), p. 352.
- <sup>34</sup>M. C. Marchetti and D. R. Nelson, *Phys. Rev. B* **42**, 9938 (1990); *Physica C* **174**, 40 (1991).
- <sup>35</sup>E. H. Brandt, *J. Low Temp. Phys.* **26**, 709 (1977); **26**, 735 (1977); **28**, 263 (1977); **28**, 291 (1977).
- <sup>36</sup>J. R. Clem, *Physica C* **153-155**, 50 (1988); I. Morgenstern, *IBM J. Res. Develop.* **33**, 307 (1989).
- <sup>37</sup>D. Dimos, P. Chaudhari, and J. Mannhart, *Phys. Rev. B* **41**, 4038 (1990).
- <sup>38</sup>M. Daeumling, J. M. Sentjens, and D. C. Larbalestier, *Nature (London)* **346**, 332 (1990); S. E. Babcock, X. Y. Cai, D. L. Kaiser, and D. C. Larbalestier, *ibid.* **347**, 167 (1990).
- <sup>39</sup>H. Kupfer, I. Apfelstedt, R. Flukiger, C. Keller, R. Meier-Hirmer, B. Runtsch, A. Turovski, U. Wiech, and T. Wolf, *Cryogenics* **29**, 225 (1989); C. Keller, H. Kupfer, R. Meier-Hirmer, U. Wiech, V. Selvamanickam, and K. Salama, *ibid.* **30**, 400 (1990); **30**, 411 (1990).
- <sup>40</sup>P. C. Hohenberg and B. I. Halperin, *Rev. Mod. Phys.* **49**, 435 (1977).
- <sup>41</sup>G. F. Mazenko, *Phys. Rev. B* **43**, 5747 (1991).
- <sup>42</sup>L. D. Landau and E. M. Lifshitz, *Fluid Mechanics* (Pergamon, Oxford, 1959).
- <sup>43</sup>D. Bensimon, L. P. Kadanoff, S. Liang, B. I. Shraiman, and C. Tang, *Rev. Mod. Phys.* **58**, 977 (1986).
- <sup>44</sup>J. S. Langer, *Rev. Mod. Phys.* **52**, 1 (1980).
- <sup>45</sup>A. M. Campbell and J. E. Evetts, *Adv. Phys.* **21**, 199 (1972).
- <sup>46</sup>M. Tashiki and S. Takahashi, *Solid State Commun.* **70**, 291 (1989); **72**, 1083 (1989).
- <sup>47</sup>P. L. Gammel, L. F. Schneemeyer, J. V. Waszczak, and D. J. Bishop, *Phys. Rev. Lett.* **61**, 1666 (1988).
- <sup>48</sup>D. E. Farrell, J. P. Rice, and D. M. Ginsberg, *Phys. Rev. Lett.* **67**, 1165 (1991).
- <sup>49</sup>E. H. Brandt, P. Esquinazi, and G. Weiss, *Phys. Rev. Lett.* **62**, 2330 (1989); A. Gupta, P. Esquinazi, H. F. Braun, and H. W. Neumuller, *ibid.* **63**, 1869 (1989); J. Klober, A. Gupta, P. Esquinazi, H. F. Braun, and E. H. Brandt, *ibid.* **66**, 2507 (1991).
- <sup>50</sup>Y. Xu and M. Suenaga, *Phys. Rev. B* **43**, 5516 (1991).
- <sup>51</sup>G. Deutscher and K. A. Muller, *Phys. Rev. Lett.* **59**, 1745 (1988).
- <sup>52</sup>I. S. Gradshteyn and I. M. Ryzhik, *Tables of Integrals, Series and Products* (Academic, New York, 1965).
- <sup>53</sup>A. Gurevich, *Supercond. Sci. Technol.* **5**, S386 (1992).
- <sup>54</sup>A. V. Gurevich, R. G. Mints, and A. L. Rakhmanov, *Physics of Composite Superconductors* (Nauka, Moscow, 1987).
- <sup>55</sup>M. V. Feigel'man, V. B. Geshkenbein, and V. M. Vinokur, *Phys. Rev. B* **43**, 6263 (1991).
- <sup>56</sup>A. Gurevich, H. Kupfer, B. Runtsch, R. Meier-Hirmer, D. Lee, and K. Salama, *Phys. Rev. B* **44**, 12090 (1991).
- <sup>57</sup>L. Fruchter, C. Aguillon, I. A. Campbell, and B. Keszei, *Phys. Rev. B* **42**, 2627 (1990).
- <sup>58</sup>Liwen Liu, J. S. Kouvel, and T. O. Brun, *Phys. Rev. B* **43**, 7859 (1991).